age distribution of the subjects,[40,42] the method of evaluating periodontitis,[11] and study design.[13]

Our study found a relationship between periodontitis and ECG abnormalities, which suggests a relationship between periodontitis and CVD. Known risk factors for CVD, such as blood pressure, smoking status, alcohol consumption, and exercise frequency were also related to ECG abnormalities in the bivariate analyses; however, only periodontal condition, systolic blood pressure, and age were significant after the multivariate adjustment. The reported relative contribution of periodontitis to risk of CVD is generally small. In order to examine the degree of cardiovascular risk from periodontitis as compared to other risk factors, stringently designed cohort studies are required. Clinical intervention studies that examine whether treatment of periodontal disease reduces the risk of CVD will produce an answer.

ACKNOWLEDGMENTS

The authors respectfully dedicate this paper to the memory of Toshihiko Koga, who died October 14, 2001. We are grateful to Dr. Daisuke Ikeda and Atsusi Hideshima, Kyushu University, Fukuoka, Japan, for assisting in the oral examination. This work was supported in part by Grant-in-Aid of Scientific Research (B) 15390652 (T. S.) from the Ministry of Education, Science, Sports and Culture of Japan.

REFERENCES

1. DeStefano F, Anda RF, Kahn HS, Williamson DF, Russell CM. Dental disease and risk of coronary heart disease and mortality. *Br Med J* 1993;306:688-691.
2. Beck J, Garcia R, Heiss G, Vokonas PS, Offenbacher S. Periodontal disease and cardiovascular disease. *J Periodontol* 1996;67:1123-1137.
3. Beck JD, Pankow J, Tyroler HA, Offenbacher S. Dental infections and atherosclerosis. *Am Heart J* 1999; 138(Suppl.):S528-S533.
4. Emingil G, Buduneli E, Aliyev A, Akilli A, Atilla G. Association between periodontal disease and acute myocardial infarction. *J Periodontol* 2000;71:1882-1886.
5. Lopez R, Oyarzun M, Naranjo C, Ortiz M, Baelum V. Coronary heart disease and periodontitis-a case control study in Chilean adults. *J Clin Periodontol* 2002;29:468-473.
6. Genco R, Offenbacher S, Beck J. Periodontal disease and cardiovascular disease: Epidemiology and possible mechanisms. *J Am Dent Assoc* 2002;133(Suppl.):14S-22S.
7. Danesh J, Collins R, Peto R. Chronic infections and coronary heart disease: Is there a link? *Lancet* 1997;350: 430-436.
8. Patel P, Mendall MA, Carrington D, et al. Association of *Helicobacter pylori* and *Chlamydia pneumoniae* infections with coronary heart disease and cardiovascular risk factors. *Br Med J* 1995;311:711-714.
9. Chiu B. Multiple infections in carotid atherosclerotic plaques. *Am Heart J* 1999;138(Suppl.):S534-S536.
10. Haraszthy VI, Zambon JJ, Trevisan M, Zeid M, Genco RJ. Identification of periodontal pathogens in atheromatous plaques. *J Periodontol* 2000;71:1554-1560.
11. Howell TH, Ridker PM, Ajani UA, Hennekens CH, Christian WG. Periodontal disease and risk of subsequent cardiovascular disease in U.S. male physicians. *J Am Coll Cardiol* 2001;37:445-450.
12. Hujoel PP, Drangsholt M, Spiekerman C, DeRouen TA. Periodontal disease and coronary heart disease risk. *JAMA* 2000;284:1406-1410.
13. Hujoel PP, Drangsholt M, Spiekerman C, DeRouen TA. Examining the link between coronary heart disease and the elimination of chronic dental infections. *J Am Dent Assoc* 2001;132:883-889.
14. Hujoel PP, Drangsholt M, Spiekerman C, DeRouen TA. Pre-existing cardiovascular disease and periodontitis: A follow-up study. *J Dent Res* 2002;81:186-191.
15. Danesh J. Coronary heart disease, *Helicobacter pylori*, dental disease, *Chlamydia pneumoniae*, and cytomegalovirus: Meta-analyses of prospective studies. *Am Heart J* 1999;138(Suppl.):S434-S437.
16. Cedres BL, Liu K, Stamler J, et al. Independent contribution of electrocardiographic abnormalities to risk of death from coronary heart disease, cardiovascular diseases and all causes. Findings of three Chicago epidemiologic studies. *Circulation* 1982;65:146-153.
17. Knutsen R, Knutsen SF, Curb JD, Reed DM, Kautz JA, Yano K. The predictive value of resting electrocardiograms for 12-year incidence of coronary heart disease in the Honolulu Heart Program. *J Clin Epidemiol* 1988; 41:293-302.
18. Blackburn H, Taylor HL, Keys A. Coronary heart disease in seven countries. XVI. The electrocardiogram in prediction of five-year coronary heart disease incidence among men aged forty through fifty-nine. *Circulation* 1970;41: 1154-1161.
19. Gordon T, Kannel WB. Premature mortality from coronary heart disease. The Framingham study. *JAMA* 1971; 215:1617-1625.
20. Rose G, Baxter PJ, Reid DD, McCartney P. Prevalence and prognosis of electrocardiographic findings in middle-aged men. *Br Heart J* 1978;40:636-643.
21. Castelli WP. Cardiovascular disease and multifactorial risk: Challenge of the 1980s. *Am Heart J* 1983;106:1191-1200.
22. Kagan A, Yano K, Reed DM, MacLean CJ. Predictors of sudden cardiac death among Hawaiian-Japanese men. *Am J Epidemiol* 1989;130:268-277.
23. Ichihara Y, Sugino M, Hattori R, et al. Relation of electrocardiographic left ventricular hypertrophy with and without T-wave changes to systemic blood pressure, body mass, and serum lipids and blood glucose levels in Japanese men. *Am J Cardiol* 1997;80:730-735.
24. Menotti A, Seccareccia F. Electrocardiographic Minnesota code findings predicting short-term mortality in asymptomatic subjects. The Italian RIFLE Pooling Project (Risk Factors and Life Expectancy). *G Ital Cardiol* 1997;27:40-49.
25. De Bacquer D, De Backer G, Kornitzer M, Blackburn H. Prognostic value of ECG findings for total, cardiovascular disease, and coronary heart disease death in men and women. *Heart* 1998;80:570-577.
26. Tanizaki Y, Kiyohara Y, Kato I, et al. Incidence and risk factors for subtypes of cerebral infarction in a general population: The Hisayama study. *Stroke* 2000;31:2616-2622.
27. Brown LJ, Brunelle JA, Kingman A. Periodontal status in the United States, 1988-1991: Prevalence, extent, and demographic variation. *J Dent Res* 1996;75(Spec. Issue): 672-683.
28. Albandar JM, Brunelle JA, Kingman A. Destructive periodontal disease in adults 30 years of age and older in the United States, 1988-1994. *J Periodontol* 1999;70: 13-29.

29. Silness J, Löe H. Periodontal disease in pregnancy. II. Correlation between oral hygiene and periodontal condition. *Acta Odontol Scand* 1964;22:121-135.
30. Pipberger HV, Simonson E, Lopez EA Jr., Araoye MA, Pipberger HA. The electrocardiogram in epidemiologic investigations. A new classification system. *Circulation* 1982;65:1456-1464.
31. Saito T, Murakami M, Shimazaki Y, Oobayashi K, Matsumoto S, Koga T. Association between alveolar bone loss and elevated serum C-reactive protein in Japanese men. *J Periodontol* 2003;74:1741-1746.
32. Loos BG, Craandijk J, Hoek FJ, Wertheim-vanDillen PM, van der Velden U. Elevation of systemic markers related to cardiovascular diseases in the peripheral blood of periodontitis patients. *J Periodontol* 2000;71:1528-1534.
33. Herzberg MC, Meyer MW. Effects of oral flora on platelets: Possible consequences in cardiovascular disease. *J Periodontol* 1996;67:1138-1142.
34. Herzberg MC, Meyer MW. Dental plaque, platelets, and cardiovascular diseases. *Ann Periodontol* 1998;3:151-160.
35. Sharma A, Novak EK, Sojar HT, Swank RT, Kuramitsu HK, Genco RJ. *Porphyromonas gingivalis* platelet aggregation activity: Outer membrane vesicles are potent activators of murine platelets. *Oral Microbiol Immunol* 2000;15:393-396.
36. Genco RJ, Trevisan M, Wu T, Beck JD. Periodontal disease and risk of coronary heart disease [letter to the editor]. *JAMA* 2001;285:40-41.
37. Morrison HI, Ellison LF, Taylor GW. Periodontal disease and risk of fatal coronary heart and cerebrovascular diseases. *J Cardiovasc Risk* 1999;6:7-11.
38. Slade GD, Offenbacher S, Beck JD, Heiss G, Pankow JS. Acute-phase inflammatory response to periodontal disease in the US population. *J Dent Res* 2000;79:49-57.
39. Papapanou PN, Wennström JL, Johnsson T. Extent and severity of periodontal destruction based on partial clinical assessments. *Community Dent Oral Epidemiol* 1993; 21:181-184.
40. Takata Y, Ansai T, Matsumura K, et al. Relationship between tooth loss and electrocardiographic abnormalities in octogenarians. *J Dent Res* 2001;80:1648-1652.
41. Joshipura KJ, Rimm EB, Douglass CW, Trichopoulos D, Ascherio A, Willett WC. Poor oral health and coronary heart disease. *J Dent Res* 1996;75:1631-1636.
42. Mattila KJ, Asikainen S, Wolf J, Jousimies-Somer H, Valtonen V, Nieminen M. Age, dental infections, and coronary heart disease. *J Dent Res* 2000;79:756-760.

Correspondence: Dr. Yoshihiro Shimazaki, Department of Preventive Dentistry, Kyushu University Faculty of Dental Science, 3-1-1 Maidashi, Higashi-ku, Fukuoka 812-8582, Japan. Fax: 81-92-642-6354; e-mail: shimadha@mbox.nc.kyushu-u.ac.jp.

Accepted for publication October 24, 2003.

Published online November 5, 2004

5928–5934 *Nucleic Acids Research, 2004, Vol. 32, No. 19*
doi:10.1093/nar/gkh909

Futile short-patch DNA base excision repair of adenine:8-oxoguanine mispair

Keiji Hashimoto, Yohei Tominaga[1], Yusaku Nakabeppu[1] and Masaaki Moriya*

Laboratory of Chemical Biology, Department of Pharmacological Sciences, State University of New York, Stony Brook, NY 11794-8651, USA and [1]Division of Neurofunctional Genomics, Department of Immunobiology and Neuroscience, Medical Institute of Bioregulation, Kyushu University, Fukuoka 812-8582, Japan

Received September 30, 2004; Accepted October 7, 2004

ABSTRACT

8-Oxo-7, 8-dihydrodeoxyguanosine (8-oxo-dG), one of the representative oxidative DNA lesions, frequently mispairs with the incoming dAMP during mammalian DNA replication. Mispaired dA is removed by post-replicative base excision repair (BER) initiated by adenine DNA glycosylase, MYH, creating an apurinic (AP) site. The subsequent mechanism ensuring a dC:8-oxo-dG pair, a substrate for 8-oxoguanine DNA glycosylase (OGG1), remains to be elucidated. At the nucleotide insertion step, none of the mammalian DNA polymerases examined exclusively inserted dC opposite 8-oxo-dG that was located in a gap. AP endonuclease 1, which possesses 3′→5′ exonuclease activity and potentially serves as a proofreader, did not discriminate dA from dC that was located opposite 8-oxo-dG. However, human DNA ligases I and III joined 3′-dA terminus much more efficiently than 3′-dC terminus when paired to 8-oxo-dG. In reconstituted short-patch BER, repair products contained only dA opposite 8-oxo-dG. These results indicate that human DNA ligases discriminate dC from dA and that MYH-initiated short-patch BER is futile and hence this BER must proceed to long-patch repair, even if it is initiated as short-patch repair, through strand displacement synthesis from the ligation-resistant dC terminus to generate the OGG1 substrate, dC:8-oxo-dG pair.

INTRODUCTION

The integrity of genomic DNA is maintained by accurate DNA replication and elaborate DNA repair in living cells. Among various threats to genetic information, oxidative damage to DNA is most abundant and inevitable as cells produce reactive oxygen species through energy metabolism (1). One of the oxidative DNA lesions, 8-oxo-7, 8-dihydrodeoxyguanosine (8-oxo-dG), is deleterious as it frequently mispairs with the incoming dAMP during DNA replication (2), leading to G:C→T:A transversions (3,4). Adenine paired to 8-oxo-dG is recognized and removed by adenine DNA glycosylase, MYH (MUTYH), a mammalian homolog of bacterial MutY (5,6). Recently, it was reported that inherited defects in the human *MYH* gene were associated with multiple colorectal tumors and somatic G→T mutations in the adenomatous polyposis coli (*APC*) gene (7). Furthermore, knockout of the mouse *MYH* gene resulted in spontaneous cancer (8) and a mutator phenotype in embryonic stem cells (9). These pieces of evidence emphasize the importance of the MYH-initiated base excision repair (BER) in cancer/mutation avoidance.

MYH is an adenine DNA glycosylase and initiates post-replication BER by removing adenine residues from DNA when paired to 8-oxo-dG or dG (5,6). Apurinic (AP) sites generated by MYH glycosylase is cleaved by AP endonuclease (APE), generating 3′-OH and 5′-deoxyribose phosphate (dRP). The 3′-OH residue serves as a primer terminus for a repair synthesis. When short-patch BER proceeds, 1 nt gap is converted to a nick by the actions of gap-filling DNA polymerase (pol) and deoxyribophosphodiesterase (dRPase). When long-patch BER proceeds, a strand displacement synthesis and the excision of a displaced strand by flap-endonuclease 1 (FEN1, DNase IV) are required to produce a ligatable nick (6,10). In both the cases, ligation of the nick follows to complete repair reactions. In BER of 8-oxo-dG:dA to 8-oxo-dG:dC, the mechanism following the removal of adenine base is not understood well. Unlike regular BER, the DNA glycosylase, MYH, removes the undamaged base, adenine, and DNA polymerase inserts a nucleotide opposite the lesion, 8-oxo-dG. The reactions must ensure the formation of 8-oxo-dG:dC pair, which is then repaired to dG:dC by regular BER initiated by 8-oxoguanine DNA glycosylase (OGG1). MYH is located in replication foci (11) and interacts with the proliferating cell nuclear antigen (PCNA), APE1, MSH6 and RPA (12,13). The post-replication repair is coupled with replication (14) and is suggested to follow long-patch BER (12,15,16). However, even if the long-patch BER is the mechanism for the repair, the reason for this choice is not clear. It is plausible that 8-oxo-dG inhibits ligation of a nucleotide inserted opposite this lesion during short-patch BER, hence the repair proceeds to the long-patch repair pathway.

To gain insights into the post-replication repair, we examined the three steps (nucleotide insertion, proofreading and ligation) that are involved in the repair. We also reconstituted short-patch BER of 8-oxo-dG:dA with purified proteins.

*To whom correspondence should be addressed. Tel: +1 631 444 3082; Fax: +1 631 444 7641; Email: maki@pharm.sunysb.edu

MATERIALS AND METHODS

Enzymes

Mouse MYH was purified as described previously (9). Human APE1, PCNA and calf thymus DNA polymerase δ were provided by Carlos de los Santos, Paul Fisher and Holly Miller (SUNY at Stony Brook), respectively. Human DNA polymerases, pol λ, pol η, pol κ, pol β and pol ι, were provided by Luis Blanco (Universidad Autonoma), Fumio Hanaoka (Osaka University), Haruo Ohmori (Kyoto University), Holly Miller (SUNY) and Roger Woodgate (NIH), respectively. Human DNA ligases I and IIIβ were provided by Alan Tomkinson (University of Maryland Medicine).

Expression and purification of human X-ray repair cross complementing 1 (XRCC1) and DNA ligase IIIα

Plasmids expressing histidine-tagged human XRCC1 (17) and DNA ligase IIIα (18) were provided by Larry Thompson (Lawrence Livermore National Laboratory) and Tomas Lindahl (Cancer Research UK), respectively. *Escherichia coli* BL21-CodonPlus(DE3)-RIL (Stratagene) was transformed and the protein expression was induced by the addition of isopropyl β-D-1-thiogalactopyranoside at 1 mM. After 2 h incubation at 37°C, bacteria were harvested and suspended in a buffer consisting of 50 mM Tris–HCl (pH 7.5), 10% glycerol, 0.5 M NaCl, 5 mM 2-mercaptoethanol and 1 mM imidazole. Bacteria were sonicated and a crude extract was obtained by ultracentrifugation. The extract was applied to a Ni-NTA agarose column (QIAGEN), and the column was washed successively with 1, 40 and 80 mM imidazole-containing buffers. XRCC1 and DNA ligase IIIα proteins were eluted with a 250 mM imidazole-containing buffer. Identity and purity of proteins were confirmed by SDS–PAGE. Proteins were dialyzed against a buffer containing 50 mM Tris–HCl (pH 7.5), 50% glycerol, 0.1 M NaCl, 1 mM EDTA and 10 mM 2-mercaptoethanol and then stored at −20°C. Protein concentration was determined with Protein Assay reagent (BioRad) using BSA as a standard.

Oligonucleotides

All oligonucleotides were synthesized by the DNA synthesis facility (SUNY, Stony Brook) and purified by electrophoresis in a denaturing 20% polyacrylamide gel. 5′-End labeling was carried out using [γ-^{32}P]ATP (3000 Ci/mmol, Amersham Biosciences) and T4 polynucleotide kinase (New England BioLabs). Labeled oligonucleotides were purified by a Micro-Spin G-25 column (Amersham Biosciences). For the preparation of duplex DNA, oligonucleotides were incubated at 80°C for 10 min in a solution (50 μl) containing 0.1× TE and 100 mM NaCl and then slowly cooled to room temperature.

Template oligonucleotides (40mer) were 5′CCAACTTG-AAAACGCTCCACXATACCTTACATGCTAGAAC where X = dG or 8-oxo-dG. For nucleotide insertion experiments, 5′-^{32}P-labeled 19mer primer (5′GTTCTAGCATGTAAG-GTAT) and 5′-phosphorylated downstream 20mer oligonucleotide (5′GTGGAGCGTTTTCAAGTTGG) were annealed to template 40mer, forming a 1 nt gap in the middle of duplex DNA. For DNA ligation and exonuclease assays, 5′-^{32}P-labeled 20mer oligonucleotides (5′GTTCTAGCATGTAAG-GTATX, where X = dA, dC, dG or dT) and 5′-phosphorylated downstream 20mer oligonucleotide (described above) were annealed to template 40mer, generating a substrate with a correctly paired or mispaired 3′ terminus at a nick in the middle of duplex DNA. For MYH-initiated reconstitution experiments, dA:8-oxo-dG mispair-containing 40mer/40mer duplex DNA was employed.

Nucleotide insertion reaction

The reaction mixture (20 μl) contained 50 mM Tris–HCl (pH 7.5), 5 mM $MgCl_2$, 30 mM KCl, 5 mM DTT, 100 μg/ml BSA, 25 nM 5′-labeled primer/template, 2.5 nM enzyme (pol β, pol η, pol ι, pol κ or pol λ) and dATP or dCTP (concentrations are indicated in Figure 1). For reactions with pol δ, the mixture (20 μl) contained 40 mM bis-Tris (pH 6.7), 6 mM $MgCl_2$, 10 mM DTT, 250 μg/ml BSA, 25 nM 5′-labeled primer/template, 110 nM PCNA (as a trimer), 2.25 U pol δ and dATP or dCTP. For reaction containing both dATP and dCTP, the mixture (20 μl) contained 50 mM Tris–HCl (pH 7.5), 5 mM $MgCl_2$, 30 mM KCl, 10 mM DTT, 250 μg/ml BSA, 25 nM unlabeled primer/template, 2.5 nM enzyme (pol β, pol η or pol λ), 0.5 μM dATP, 0.5 μM dCTP and 6.6 nM (3000 Ci/mmol) of [α-^{32}P]dATP or [α-^{32}P]dCTP. The reaction was conducted at 37°C for 10 min and terminated by adding 20 μl of a formamide loading buffer (96% formamide, 0.1% bromophenol blue, 0.1% xylene cyanol, 19 mM EDTA) followed by heating at 90°C for 3 min. The products were analyzed by electrophoresis in a denaturing 20% polyacrylamide gel. Radioactive DNA bands were visualized and quantified by a Storm840 PhosphorImager and ImageQuant software (Amersham Biosciences).

Assay for 3′→5′ exonuclease activity of APE1

The reaction mixture (20 μl) contained 50 mM Tris–HCl (pH 7.5), 5 mM $MgCl_2$, 30 mM KCl, 5 mM DTT, 50 μg/ml BSA, 10 nM 5′-labeled substrate and 0, 1 or 5 nM APE1. The reaction was performed at 37°C for 30 min and terminated as described above.

DNA ligation reaction

The reaction mixture (20 μl) contained 50 mM Tris–HCl (pH 7.5), 5 mM $MgCl_2$, 5 mM DTT, 1 mM ATP, 50 μg/ml BSA, 100 mM KCl, 10 nM 5′-labeled substrate and human DNA ligases I (0, 5 and 25 nM), IIIα (0, 0.5 and 2.5 nM) or IIIβ (0, 5 and 25 nM). The ligation mixture was incubated at 37°C for 30 min, after which products were analyzed by gel electrophoresis as described above. In time-course experiments (Figure 4), 50 nM DNA ligase I or 10 nM DNA ligase IIIα/XRCC1 was used in 200 μl of the reaction mixture containing 2 mM ATP (instead of 1 mM) and 0 or 150 mM KCl. Aliquots (10 μl) were removed at various time points during incubation at 37°C, quenched and analyzed for products as described above.

Adenine base excision catalyzed by MYH and APE1

The reaction mixture (20 μl) contained 50 mM Tris–HCl (pH 7.5), 5 mM $MgCl_2$, 5 mM DTT, 50 μg/ml BSA, 1 nM 5′-labeled 40mer duplex DNA and MYH (0, 2.5, 5 or 10 nM) and was incubated at 37°C for 15 min followed by incubation with APE1 (0, 10 or 50 nM) in the presence of 150 mM KCl at 37°C for 15 min (Figure 5).

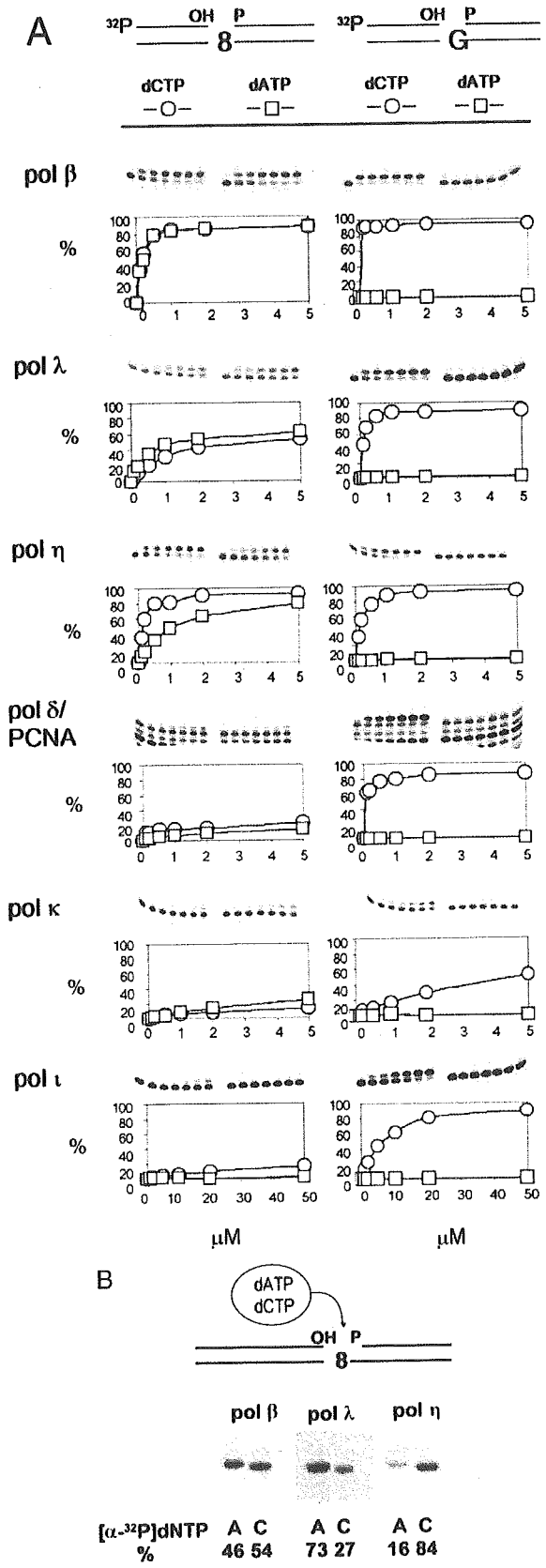

Figure 1. Nucleotide insertion opposite 8-oxo-dG. (**A**) Insertion of dAMP or dCMP opposite 8-oxo-dG was determined using 40mer duplex DNA that had a 1 nt gap opposite the lesion. Substrate DNA is shown on the top. Here, '8' stands for 8-oxo-dG. Intensities of radioactive bands were measured and insertion frequency, represented as percent, was plotted as a function of nucleotide concentration (μM). (**B**) Nucleotide insertion was determined in the presence of both 0.5 μM dATP and 0.5 μM dCTP. Either [α-^{32}P]dATP or [α-^{32}P]dCTP was included in the reaction mixture as a tracer. Relative ratio of insertions of dAMP and dCMP was shown in percentage.

Reconstitution of MYH-initiated short-patch BER

A starting reaction mixture (100 μl) contained 1 nM unlabeled 40mer duplex DNA and 10 nM MYH and was incubated at 37°C for 30 min. Following the reaction, the mixture was supplemented with 150 mM KCl, 2 mM ATP, 0.5 μM dATP, 0.5 μM dCTP and 33 nM of [α-^{32}P]dATP or [α-^{32}P]dCTP (6000 Ci/mmol), 100 nM APE1, 4 nM pol β and 10 nM of DNA ligase IIIα/XRCC1, and then incubated at 37°C. Aliquots (10 μl) were removed at various time points and the products were analyzed as described above.

RESULTS

Both dAMP and dCMP are inserted opposite 8-oxo-dG by various DNA polymerases

The consecutive action of MYH and APE1 produces a 1 nt gap opposite 8-oxo-dG with 3′-OH group and 5′-dRP moiety, and 8-oxo-dG serves as a template for the repair synthesis. We examined the insertion specificity of several DNA polymerases using a 1 nt gapped substrate (Figure 1A and B). Among DNA polymerases examined, pol β, pol η and pol λ inserted a nucleotide opposite 8-oxo-dG more efficiently than do pol κ, pol ι and pol δ/PCNA. Regarding their specificities, pol η and its close relative, pol ι, preferred dC to dA; pol β and pol δ/PCNA appeared to insert dC and dA at similar frequencies; and pol λ and pol κ preferred dA to dC. All these pols inserted dC opposite dG (Figure 1A) though the activities of pol κ and pol ι were weak when a gapped substrate was used. These results indicate that none of the DNA polymerases exclusively inserts dC opposite 8-oxo-dG.

APE1 exonuclease activity does not discriminate dA from dC pairing to 8-oxo-dG

APE1 is reported to have a 3′→5′ exonuclease activity active on 3′-mismatched termini of nicked and gapped DNA molecules and is suggested to compensate for the lack of a proofreading function of pol β (19). This finding raises the possibility that APE1 removes selectively 3′-dA, but not dC, inserted opposite 8-oxo-dG during a gap-filling reaction. To explore this possibility, we used four substrates with different termini at nicks (Figure 2). When dG was a template, all mismatched termini, but not 3′-dC, were subjected to proofreading. When 8-oxo-dG was a template, all four termini were proofread: there was no difference between 3′-dC and 3′-dA, and this result was true under three different KCl concentrations (0, 30 and 150 mM). The exonuclease activity of APE1 was progressively impaired by KCl. We conclude that APE1 does not discriminate 3′-dA from 3′-dC inserted opposite 8-oxo-dG.

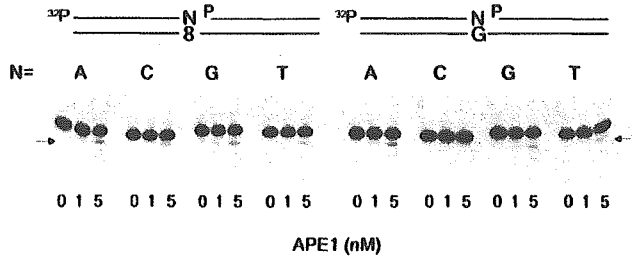

Figure 2. 3′→5′ Exonucleolytic proofreading activity of APE1. Nicked DNA substrate is shown above the panel. 'N' stands for dA, dC, dG or dT. Arrows indicate proofread products.

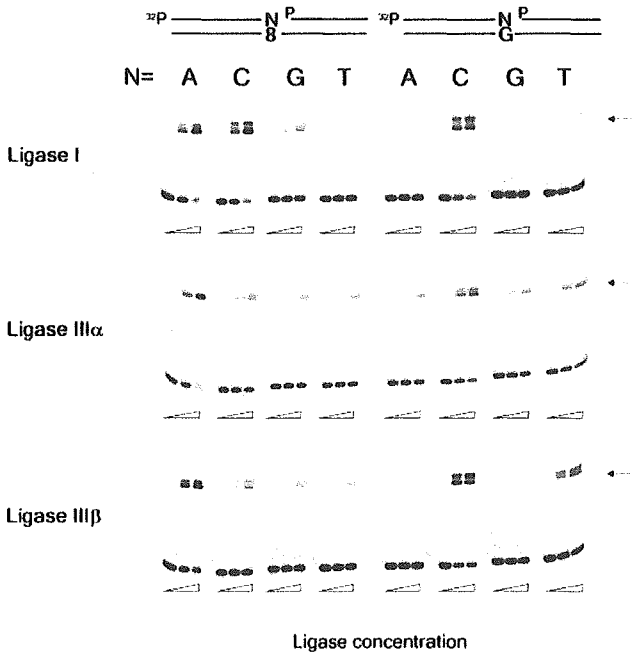

Figure 3. Ligation of four 3′-termini pairing with 8-oxo-dG or dG to downstream DNA. Nicked DNA substrate is shown on the top. Ligation products are 40mer indicated by arrows. All oligonucleotides used in this study were purified by gel electrophoresis and showed one band, but ligation products always appeared as two bands. We do not know the reason for this. The concentrations of ligases were 0, 0.5 and 2.5 nM for ligase IIIα and 0, 5 and 25 nM for ligase I and IIIβ.

DNA ligases ligate 3′-dA terminus much more efficiently than 3′-dC terminus when pairing to 8-oxo-dG

If a DNA ligase is active on only 3′-dC terminus pairing to 8-oxo-dG, the ligation step will play a critical role in the short-patch BER of dA:8-oxo-dG mispair. We compared the degrees of ligation of four 3′-termini pairing to 8-oxo-dG. Human DNA ligase I, which is believed to be engaged in DNA replication, long-patch BER and nucleotide excision repair appeared to ligate both 3′-dA and 3′-dC termini at similar efficiencies in a qualitative experiment (Figure 3). The other two termini, dG and dT, were poorly ligated by this enzyme. DNA ligases IIIα and IIIβ, which are produced by an alternative splicing (20), appeared to be much more active on 3′-dA than on the other termini. When unmodified DNA

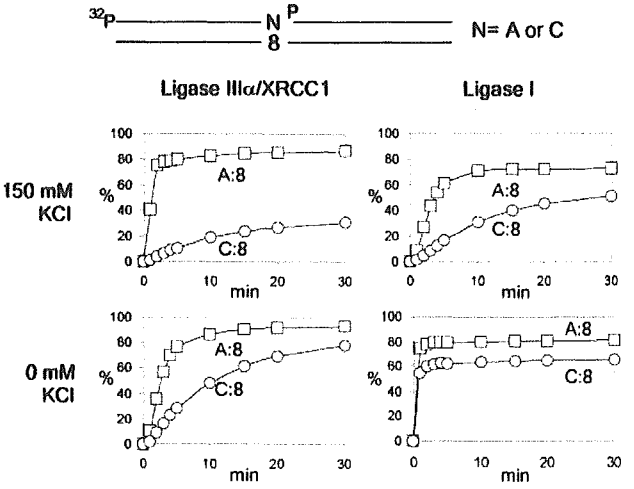

Figure 4. Time course of DNA ligation catalyzed by human DNA ligase I and ligase III/XRCC1 in the presence (150 mM) or in the absence of KCl. Substrate DNA was the same as in Figure 3, and 'N' stands for A or C. The *x*-axis and *y*-axis represent incubation time (min) and generation of ligation products (percent), respectively.

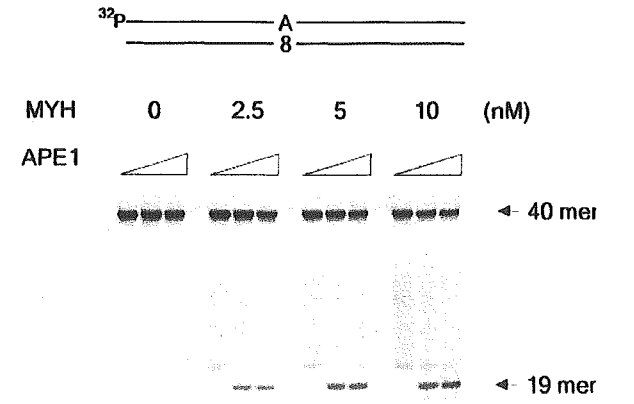

Figure 5. Adenine base excision catalyzed by MYH and APE1. 5′-Labeled duplex 40mer containing dA:8-oxo-dG pair was incubated with MYH at 37°C for 15 min followed by 15 min incubation with APE1 (0, 10 or 50 nM) in the presence of 150 mM KCl.

was used as a substrate, ligase I exclusively ligated a 3′-dC terminus pairing to dG, whereas ligases IIIα and IIIβ ligated a dT terminus as well as a dC terminus. Since DNA ligase IIIα is believed to be the ligase involved in short-patch BER, we further characterized ligation catalyzed by this enzyme of 3′-dA and 3′-dC termini pairing to 8-oxo-dG (Figure 4). Burst DNA joining occurred on the dA terminus, but not on the dC terminus, in a reaction mixture containing 150 mM KCl, which is considered to represent the physiological salt condition (21). Ligation of the dA terminus was also more efficient than that of the dC terminus in the absence of KCl, but the difference was less drastic. The effects of varying amounts of XRCC1 on the ligation of 3′-dA and -dC termini were also

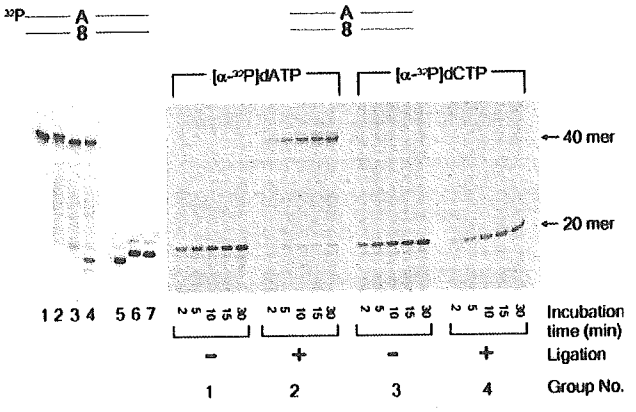

Figure 6. Reconstitution of MYH-initiated short-patch BER. Substrate DNA (duplex 40mer) is shown above the panel. Lanes 1–4 show base excision reaction catalyzed by MYH, using 5′-^{32}P-labeled substrate. Lane 1, substrate DNA; lanes 2 and 3, incubated with 10 nM MYH for 30 min (lane 2) followed by heating at 90°C for 3 min (lane 3); lane 4, incubated with MYH followed by APE1 treatment for 30 min in the presence of 150 mM KCl; lane 5, 5′-^{32}P-labeled standard 19mer corresponding to MYH/APE1-generated product; lanes 6 and 7, standard 19mer plus 3′-dA (lane 6) or 3′-dC (lane 7). All the other lanes show reconstitution reaction using [α-^{32}P]dATP or [α-^{32}P]dCTP in the presence or in the absence of ligation reaction catalyzed by DNA ligase IIIα/XRCC1.

examined, and no significant effects were observed (data not shown). The ligation catalyzed by DNA ligase I was also characterized under the same condition. Both in the presence and in the absence of 150 mM KCl, ligation of a 3′-dA terminus was more efficient than that of a dC terminus pairing to 8-oxo-dG, which was similar to the result with ligase IIIα, but the difference was less marked. We have also tested *E.coli* and T4 DNA ligases, and the results were similar to those with ligase I (data not shown). From these results, it is concluded that DNA ligases, especially human ligase IIIα, are much more active on a dA terminus than on a dC terminus pairing to 8-oxo-dG.

Adenine base excision and strand incision catalyzed by MYH and APE1

When 5′-^{32}P labeled 40mer duplex bearing a dA:8-oxo-dG pair was incubated with MYH, a faint band migrating above 19mer was detected (Figure 5). This band may be the product of β-elimination reaction of an AP site generated by MYH. When APE1 was added to this reaction mixture in the presence of 150 m KCl, a distinct band was generated. This band corresponds to 19mer with 3′-OH terminus. Thus, the combined action of MYH and APE1 generates a 1 nt gap opposite 8-oxo-dG with 3′-OH and 5′dRP termini.

Reconstitution of MYH-initiated short-patch BER of dA:8-oxo-dG mispair

So far, each step of short-patch BER was characterized individually. In this section, short-patch BER was reconstituted using purified proteins. As described in 'Materials and Methods', unlabeled duplex 40mer was first incubated with MYH, then the reaction mixture was supplemented with the other protein factors (APE1, pol β and DNA ligase IIIα/XRCC1) and co-factors (KCl, ATP, dATP, dCTP and [α-^{32}P] dATP or [α-^{32}P] dCTP). The dA (group 1) and dC (group 3) were inserted opposite 8-oxo-dG as revealed in reaction mixtures lacking the ligase (Figure 6). Although inserted dA was ligated efficiently (group 2), dC was not (group 4). These results indicate that the short-patch repair is completed only when dAMP is inserted opposite 8-oxo-dG.

DISCUSSION

8-Oxo-dG exerts its genotoxity mainly by pairing with dA during DNA replication. In *E.coli*, the frequency of this misincorporation is ~30% when measured in *mutM*$^-$*mutY*$^-$ cells, and more than 90% of these misincorporated dAs are removed by MutY-initiated post-replication repair (22). Although a misincorporation frequency of dA has not yet been determined in human cells, a similar repair process is expected to operate since MYH-defective cells are mutation-prone (9).

In this paper, we conducted biochemical studies using purified proteins to understand the mammalian post-replication repair. We focused on the short-patch BER and examined characteristics of enzymes involved in this repair. None of the mammalian DNA polymerases examined inserted exclusively dC opposite 8-oxo-dG, and mis-inserted dA was not specifically proofread by human APE1. However, at a ligation step, human DNA ligases I and III ligated a 3′-dA terminus pairing to 8-oxo-dG much more efficiently than a 3′-dC terminus. Thus, the ligation step discriminates dA from dC. In reconstitution experiments, DNA was ligated only when dA was inserted opposite 8-oxo-dG, indicating that MYH-initiated short-patch BER is futile and a dC:8-oxo-dG pair must proceed to long-patch BER to complete the repair. Our results support the previous suggestion that the long-patch pathway is responsible for this repair (12,15,16). One of the major questions about the repair of a dA:8-oxo-dG mispair is which DNA polymerase is responsible for dC insertion opposite 8-oxo-dG. In the experiments with cell extracts (15), the gap-filling synthesis step is sensitive to aphidicolin, suggesting that a replicative polymerase, pol δ/pol ε, is critical. However, it is unknown whether the aphidicolin-sensitive polymerase catalyzes both nucleotide insertion opposite 8-oxo-dG and extension. Indeed, there is a suggestion that pol β and pol δ/ε play a role in nucleotide insertion and extension steps, respectively, during a long-patch repair (23,24). Therefore, it is possible that nucleotide insertion opposite 8-oxo-dG and extension from the terminus are catalyzed by different polymerases. Furthermore, there are conflicting reports on the sensitivity of pol λ to aphidicolin (25,26). Since this polymerase possesses dRPase activity (27), it may function in short-patch BER. Therefore, we assessed mammalian DNA polymerases for their abilities to insert a nucleotide opposite 8-oxo-dG, using a gapped substrate. A widely spread idea is that 'repair' DNA polymerase preferentially inserts dC opposite 8-oxo-dG. However, none of the DNA polymerases examined exclusively inserted dC. The dRPase activity is required to complete short-patch BER. Pol β (28) and pol λ (27) have dRPase activities while the activity of pol ι is controversial (29,30). Pol β and pol λ, members of X-family polymerases, efficiently inserted both dA and dC into a 1 nt gap opposite 8-oxo-dG (Figure 1). Thus,

both enzymes are candidate DNA polymerases involved in this BER. Although pol η preferentially inserted dC, it is reported that pol η, pol κ and pol ι are covalently trapped by a 5′-dRP residue and their repair synthesis activities are greatly reduced (30). In addition, pol ι or pol κ is not very active in inserting a nucleotide opposite 8-oxo-dG. Thus, these polymerases may not be suitable for the repair synthesis. Pol δ also can insert dC and dA opposite the lesion as reported previously (31) and may be responsible for both steps. It is conceivable that a certain factor keeps 8-oxo-dG in the *anti* conformation and assists DNA polymerase to insert dC opposite 8-oxo-dG (32). However, whichever the polymerase that is responsible for the dC insertion is, short-patch BER cannot complete the post-replication repair since a dC terminus is not ligated efficiently by DNA ligases, especially by ligase III/XRCC1 that is believed to be involved in short-patch BER (6).

Our results support the previous idea that the long-patch repair is responsible for this post-replicaton repair (12,15,16). This pathway may be selected at the initiation of the repair since proteins necessary for the long-patch repair, such as MYH, PCNA, FEN1 and pol δ, are immediately available in the replication foci (11). Alternatively, it can be the result of the inhibition of short-patch repair as shown here. These two possibilities may be distinguished by identifying a polymerase that catalyzes nucleotide insertion opposite 8-oxo-dG. The possible *in vivo* roles for pol β and pol λ in this regard are currently under investigation. It is also possible that a short piece of terminal DNA downstream from the 1 nt gap opposite 8-oxo-dG is removed and a replicative, not a gap-filling, synthesis reinitiates opposite 8-oxo-dG.

ACKNOWLEDGEMENTS

We thank Luis Blanco, Carlos de los Santos, Paul Fisher, Fumio Hanaoka, Thomas Kunkel, Tomas Lindahl, Holly Miller, Haruo Ohmori, Larry Thompson, Alan Tomkinson and Roger Woodgate for enzymes and expression vectors. We also thank Cecilia Torres for oligonucleotide synthesis. This work was supported by NCI, National Institutes of Health, United States Public Health Service Grants (CA47995 and CA76163), the Ministry of Education, Culture, Sports, Science, and Technology of Japan (15025257), and the Japan Society for the Promotion of Science (15590347 and 16390119).

REFERENCES

1. Cooke,M.S., Evans,M.D., Dizdaroglu,M. and Lunec,J. (2003) Oxidative DNA damage: mechanism, mutation, and disease. *FASEB J.*, **17**, 1195–1214.
2. Shibutani,S., Takeshita,M. and Grollman,A.P. (1991) Insertion of specific bases during DNA synthesis past the oxidation-damaged base 8-oxodG. *Nature*, **349**, 431–434.
3. Wood,M.L., Dizdaroglu,M., Gajewski,E. and Essigmann,J.M. (1990) Mechanistic studies of ionizing radiation and oxidative mutagenesis: genetic effects of a single 8-hydroxyguanine (7-hydro-8-oxoguanine) residue inserted at a unique site in a viral genome. *Biochemistry*, **29**, 7024–7032.
4. Moriya,M. (1993) Single-stranded shuttle phagemid for mutagenesis studies in mammalian cells: 8-oxoguanine in DNA induces targeted G·C→T·A transversions in simian kidney cells. *Proc. Natl Acad. Sci. USA*, **90**, 1122–1126.
5. Parker,A.R. and Eshleman,J.R. (2003) Human MutY: gene structure, protein functions and interactions, and role in carcinogenesis. *Cell. Mol. Life Sci.*, **60**, 2064–2083.
6. Fortini,P., Pascucci,B., Parlanti,E., D'Errico,M., Simonelli,V. and Dogliotti,E. (2003) The base excision repair: mechanisms and its relevance for cancer susceptibility. *Biochimie*, **85**, 1053–1071.
7. Al-Tassan,N., Chmiel,N.H., Maynard,J., Fleming,N., Livingston,A.L., Williams,G.T., Hodges,A.K., Davies,D.R., David,S.S., Sampson,J.R. and Cheadle,J.P. (2002) Inherited variants of *MYH* associated with somatic G:C→T:A mutations in colorectal tumors. *Nature Genet.*, **30**, 227–232.
8. Xie,Y., Yang,H., Cunanan,C., Okamoto,K., Shibata,D., Pan,J., Barnes,D.E., Lindahl,T., McIlhatton,M., Fishel,R. and Miller,J.H. (2004) Deficiencies in mouse *myh* and *ogg1* result in tumor predisposition and G to T mutations in codon 12 of the *K-Ras* oncogene in lung tumors. *Cancer Res.*, **64**, 3096–3102.
9. Hirano,S., Tominaga,Y., Ichinoe,A., Ushijima,Y., Tsuchimoto,D., Honda-Ohnishi,Y., Ohtsubo,T., Sakumi,K. and Nakabeppu,Y. (2003) Mutator phenotype of MUTYH-null mouse embryonic stem cells. *J. Biol. Chem.*, **278**, 38121–38124.
10. Slupphaug,G., Kavli,B. and Krokan,H.E. (2003) The interacting pathways for prevention and repair of oxidative DNA damage. *Mutat. Res.*, **531**, 231–251.
11. Boldogh,I., Milligan,D., Lee,M.S., Bassett,H., Lloyd,R.S. and McCullough,A.K. (2001) hMYH cell cycle-dependent expression, subcellular localization and association with replication foci: evidence suggesting replication-coupled repair of adenine:8-oxoguanine mispairs. *Nucleic Acids Res.*, **29**, 2802–2809.
12. Parker,A., Gu,Y., Mahoney,W., Lee,S.H., Singh,K.K. and Lu,A-L. (2001) Human homolog of the MutY repair protein (hMYH) physically interacts with proteins involved in long patch DNA base excision repair. *J. Biol. Chem.*, **276**, 5547–5555.
13. Gu,Y., Parker,A., Wilson,T.M., Bai,H., Chang,D.-Y. and Lu,A-L. (2002) Human MutY homolog, a DNA glycosylase involved in base excision repair, physically and functionally interacts with mismatch repair proteins human MutS homolog 2/human MutS homolog 6. *J. Biol. Chem.*, **277**, 11135–11142.
14. Hayashi,H., Tominaga,Y., Hirano,S., McKenna,A.E., Nakabeppu,Y. and Matsumoto,Y. (2002) Replication-associated repair of adenine: 8-oxoguanine mispairs by MYH. *Curr. Biol.*, **12**, 335–339.
15. Parlanti,E., Fortini,P., Macpherson,P., Laval,J. and Dogliotti,E. (2002) Base excision repair of adenine/8-oxoguanine mispairs by an aphidicolin-sensitive DNA polymerase in human cell extracts. *Oncogene*, **21**, 5204–5212.
16. Fortini,P., Pascucci,B., Parlanti,E., D'Errico,M., Simonelli,V. and Dogliotti,E. (2003) 8-Oxoguanine DNA damage: at the crossroad of alternative repair pathways. *Mutat. Res.*, **531**, 127–139.
17. Caldecott,K.W., Tucker,J.D., Stanker,L.H. and Thompson,L.H. (1995) Characterization of the XRCC1-DNA ligase III complex *in vitro* and its absence from mutant hamster cells. *Nucleic Acids Res.*, **23**, 4836–4843.
18. Nash,R.A., Caldecott,K.W., Barnes,D.E. and Lindahl,T. (1997) XRCC1 protein interacts with one of two distinct forms of DNA ligase III. *Biochemistry*, **36**, 5207–5211.
19. Chou,K.M. and Cheng,Y.C. (2002) An exonucleolytic activity of human apurinic/apyrimidinic endonuclease on 3′ mispaired DNA. *Nature*, **415**, 655–659.
20. Mackey,Z.B., Ramos,W., Levin,D.S., Walter,C.A., McCarrey,J.R. and Tomkinson,A.E. (1997) An alternative splicing event which occurs in mouse pachytene spermatocytes generates a form of DNA ligase III with distinct biochemical properties that may function in meiotic recombination. *Mol. Cell. Biol.*, **17**, 989–998.
21. Bhagwat,A.S., Sanderson,R.J. and Lindahl,T. (1999) Delayed DNA joining at 3′ mismatches by human DNA ligases. *Nucleic Acids Res.*, **27**, 4028–4033.
22. Moriya,M. and Grollman,A.P. (1993) Mutations in the *MutY* gene of *Escherichia coli* enhance the frequency of targeted G:C→T:A transversions induced by a single 8-oxoguanine residue in single-stranded DNA. *Mol. Gen. Genet.*, **239**, 72–76.
23. Podlutsky,A.J., Dianova,I.I., Podust,V.N., Bohr,V.A. and Dianov,G.L. (2001) Human DNA polymerase β initiates DNA synthesis during long-patch repair of reduced AP sites in DNA. *EMBO J.*, **20**, 1477–1482.

24. Parlanti,E., Pascucci,B., Terrados,G., Blanco,L. and Dogliotti,E. (2004) Aphidicolin-resistant and -sensitive base excision repair in wild-type and DNA polymerase β-defective mouse cells. *DNA Repair*, **3**, 703–710.
25. Ramadan,K., Shevelev,I.V., Maga,G. and Hubscher,U. (2002) DNA polymerase λ from calf thymus preferentially replicates damaged DNA. *J. Biol. Chem.*, **277**, 18454–18458.
26. Shimazaki,N., Yoshida,K., Kobayashi,T., Toji,S., Tamai,K. and Koiwai,O. (2002) Over-expression of human DNA polymerase lambda in *E.coli* and characterization of the recombinant enzyme. *Genes Cells*, **7**, 639–651.
27. Garcia-Diaz,M., Bebenek,K., Kunkel,T.A. and Blanco,L. (2001) Identification of an intrinsic 5′-deoxyribose-5-phosphate lyase activity in human DNA polymerase λ. *J. Biol. Chem.*, **276**, 34659–34663.
28. Matsumoto,Y. and Kim,K. (1995) Excision of deoxyribose phosphate residues by DNA polymerase β during DNA repair. *Science*, **269**, 699–702.
29. Bebenek,K., Tissier,A., Frank,E.G., McDonald,J.P., Prasad,R., Wilson,S.H., Woodgate,R. and Kunkel,T.A. (2001) 5′-Deoxyribose phosphate lyase activity of human DNA polymerase ι *in vitro*. *Science*, **291**, 2156–2159.
30. Haracska,L., Prakash,L. and Prakash,S. (2003) A mechanism for the exclusion of low-fidelity human Y-family DNA polymerases from base excision repair. *Genes Dev.*, **17**, 2777–2785.
31. Einolf,H.J. and Guengerich,F.P. (2001) Fidelity of nucleotide insertion at 8-oxo-7, 8-dihydroguanine by mammalian DNA polymerase δ. Steady-state and pre-steady-state kinetic analysis. *J. Biol. Chem.*, **276**, 3764–3771.
32. Tominaga,Y., Ushijima,Y., Tsuchimoto,D., Mishima,M., Shirakawa,M., Hirano,S., Sakumi,K. and Nakabeppu,Y. (2004) MUTYH prevents OGG1 or APEX1 from inappropriately processing its substrate or reaction product with its C-terminal domain. *Nucleic Acids Res.*, **32**, 3198–3211.

Growth retardation and dyslymphopoiesis accompanied by G_2/M arrest in APEX2-null mice

Yasuhito Ide, Daisuke Tsuchimoto, Yohei Tominaga, Manabu Nakashima, Takeshi Watanabe, Kunihiko Sakumi, Mizuki Ohno, and Yusaku Nakabeppu

APEX2/APE2 is a secondary mammalian apurinic/apyrimidinic endonuclease that associates with proliferating cell nuclear antigen (PCNA), and the progression of S phase of the cell cycle is accompanied by its expression. To determine the biologic significance of APEX2, we established APEX2-null mice. These mice were about 80% the size of their wild-type littermates and exhibited a moderate dyshematopoiesis and a relatively severe defect in lymphopoiesis. A significant accumulation of both thymocytes and mitogen-stimulated splenocytes in G_2/M phase was seen in APEX2-null mice compared with the wild type, indicating that APEX2 is required for proper cell cycle progression of proliferating lymphocytes. Although APEX2-null mice exhibited an attenuated immune response against ovalbumin in comparison with wild-type mice, they produced both antiovalbumin immunoglobulin M (IgM) and IgG, indicating that class switch recombination can occur even in the absence of APEX2. (Blood. 2004;104: 4097-4103)

Introduction

Oxidation or other chemical modification of nucleotides and genomic DNA is a major threat to living organisms because the damage inflicted may cause alterations in base pairs or may block progression of DNA replication and transcription. Base excision repair (BER) is one of the major cellular defense mechanisms for eliminating damaged bases in genomic DNA.[1,2] DNA glycosylases catalyze the first step of BER by excising the damaged bases, and leave apurinic/apyrimidinic (AP) sites. Among the various mammalian DNA glycosylases, uracil DNA glycosylase (UNG) and MutY homolog (MUTYH) excise misincorporated bases during DNA replication, and both enzymes associate with proliferating cell nuclear antigen (PCNA), a scaffold protein for DNA replication machinery[3,4]; thus, both can initiate replication-associated BER.[4-7] APEX2/APE2,[8,9] a secondary mammalian AP endonuclease, is known to associate with PCNA through its PCNA-binding motif whereas the major AP endonuclease, APEX1/APE1/HAP1/REF1,[7,10-12] does not possess PCNA-binding motif. Therefore, we hypothesize that APEX2 is responsible for the incision of AP sites in replication-associated BER.[8,9] APEX1 was reported to be essential for early embryonic development in mice.[13] However, it has not yet been established that AP endonuclease activity is essential for mammals because, in addition to DNA repair, APEX1 also functions as a redox regulator of transcription factors.[12] Investigating the functions of both APEX1 and APEX2 is considered to be essential to clarify the biologic importance of AP endonuclease activities. To explore the biologic significance of APEX2 in vivo, we established APEX2-null mice.[14] We report herein that APEX2-null mice exhibit growth retardation and dyshematopoiesis accompanied by G_2/M arrest.

Materials and methods

Cell culture

Isolated mouse splenocytes were cultured in RPMI 1640 medium (Invitrogen, Carlsbad, CA) supplemented with 10% fetal bovine serum (Invitrogen), 50 μM 2-mercaptoethanol, 100 U/mL streptomycin, and 100 U/mL penicillin at 37°C in a humidified chamber with 5% CO_2. APEX2-null mouse embryo fibroblasts (MEFs) were isolated from embryos (13.5 days postcoital), and were cultured in Dulbecco modified Eagle medium supplemented with 10% heat-inactivated fetal calf serum, 100 U/mL streptomycin, and 100 U/mL penicillin at 37°C in a humidified chamber with 5% CO_2. The cells were routinely maintained by a standard 3T3 protocol, and spontaneously immortalized cell lines were thus established.

APEX2 expression plasmids

Two expression vectors for recombinant APEX2, pcDNA3.1/Hygro(+):mAPEX2 and pIRES1hyg:mAPEX2, were constructed by inserting DNA fragments encoding mouse APEX2 into the multiple cloning sites of pcDNA3.1/Hygro(+) (Invitrogen) and pIRES1hyg (Clontech, Palo Alto, CA), respectively.

From the Division of Neurofunctional Genomics, Department of Immunobiology and Neuroscience, Medical Institute of Bioregulation; the Department of Orthopedic Surgery, Graduate School of Medicine; and the Division of Molecular Immunology, Research Center for Prevention of Infectious Diseases, Medical Institute of Bioregulation, Kyushu University, Fukuoka, Japan.

Submitted April 19, 2004; accepted August 2, 2004. Prepublished online as *Blood* First Edition Paper, August 19, 2004; DOI 10.1182/blood-2004-04-1476.

Supported by grants from CREST, Japan Science and Technology Agency, the Ministry of Education, Culture, Sports, Science, and Technology of Japan (no. 15025257) and the Japan Society for the Promotion of Science (nos. 15590347 and 16390119).

Y.I. and D.T. contributed equally to this study.

Reprints: Daisuke Tsuchimoto, Division of Neurofunctional Genomics, Medical Institute of Bioregulation, Kyushu University, 3-1-1 Maidashi, Higashi-ku, Fukuoka 812 8582, Japan; e-mail: daisuke@bioreg.kyushu-u.ac.jp.

The publication costs of this article were defrayed in part by page charge payment. Therefore, and solely to indicate this fact, this article is hereby marked "advertisement" in accordance with 18 U.S.C. section 1734.

Establishment of APEX2-null mice

Apex2-disrupted mice were established as described previously.[14] Genotypes were analyzed by Southern blotting or by polymerase chain reaction (PCR) with the use of mouse tail DNA. PCR primers used to detect the wild-type allele were as follows: U796M, 5′GCAAGGCATCTCAACTATGGCTC3′; and L1321, 5′CTTCTCATCTTTGGACTCTGG3′. Mp2-5, 5′CTACGCATCGGTAATGAAGG3′, and L1321 were used to detect mutated allele. All primers were purchased from Hokkaido System Science (Sapporo, Japan). APEX2 protein was detected by Western blotting with the use of a specific antibody as described under "Western blotting." Heterozygous female *(Apex2$^{+/-}$)* mice were backcrossed with C57BL/6J males *(Apex2$^{+/Y}$)*. F_9 or F_{10} male mice were used in most experiments unless stated otherwise in the text. APEX2-null female mice were obtained among offspring of *Apex2* knock-out (KO) male mice and *Apex2$^{+/-}$* female mice. All mice were maintained in an air-conditioned, light time-controlled, specific-pathogen–free room. The handling and killing of the animals were in accordance with the national prescribed guidelines, and ethical approval for the studies was granted by the Animal Experiment Committee of Kyushu University (Fukuoka, Japan).

Western blotting of APEX2

Cells were suspended in extract buffer (125 mM Tris-HCl [tris(hydroxymethyl)aminomethane–HCl], pH 6.8; 2% sodium dodecyl sulfate [SDS]; 5% glycerol) and disrupted by sonication. Cell lysates were then centrifuged at 100 000*g*. Protein concentrations of supernatant were analyzed by means of a DC Protein Assay Kit (Bio-Rad Laboratories, Mississauga, ON, Canada), and 25 μg protein per lane was subjected to SDS–polyacrylamide gel electrophoresis (SDS-PAGE) and Western blotting analysis with the use of anti-mAPEX2.

Body and organ weight analysis

All mice were measured for body weight 10 times simultaneously without anesthesia, and the mean value was calculated. To measure organ weights, mice were dissected under pentobarbital anesthesia (75 mg/kg), and abdominal vessels were cut for blood drainage. Each organ was carefully removed and immediately measured.

Thymocytes, splenocytes, and bone marrow cells

Thymus and spleen were ground with glass slides, and cells were suspended in ice-cold phosphate-buffered saline (PBS) or culture medium. Bone marrow cells were suspended in ice-cold PBS by means of a syringe with a needle. An aliquot of cell suspension was diluted, and cells were counted under a microscope. The remaining cells were subjected to other analyses.

Cell cycle analysis

Flow cytometric analysis of the cell cycle was performed as previously described.[15] The cells were prepared by Nonidet P40 (NP40) treatment for the naked nuclei preparation. Then, 1×10^6 cells were centrifuged, washed with PBS, and suspended in fluorescence-activated cell sorter (FACS) buffer containing 3.4 mM sodium citrate, 10 mM NaCl, 0.1% NP40, and 50 μg/mL propidium iodide for 1 hour at 4 °C The data were analyzed by CellQuest and ModFit software (Becton Dickinson, San Jose, CA).

X-ray irradiation

Mice were irradiated with an MBR-1520R x-ray generator (Hitachi, Kashiwa, Chiba, Japan) mounted with a 1.0-mm aluminum filter. For cell count and thymocyte survival analysis, mice were irradiated at 0, 0.5, 1.0, 2.0, or 4.0 Gy and killed 21 hours after the irradiation. For cell cycle analysis, mice were irradiated at 0.5 Gy and killed 3 hours after irradiation. Thymocytes were collected, fixed with 70% of ethanol, and subjected to an analysis of DNA content.

Analysis of blood cells

Peripheral blood was collected from an axillary artery and promptly diluted with the same volume of PBS supplemented with 0.2% of EDTA-3K ([ethylenediaminetetraacetic acid]–3K). Densities of white blood cells, red blood cells, and platelets in peripheral blood were analyzed with a K-4500 hematology analyzer (Sysmex, Kobe, Japan). Surface marker molecules on peripheral white blood cells, thymocytes, and bone marrow cells were analyzed by means of an LSR flow cytometer (Becton Dickinson) after immunostaining with specific antibodies conjugated to fluorescent dye and treated with OptiLyse B reagent (Beckman Coulter, Hialeah, FL).

Transfection and establishment of stable transfectants of MEFs

Three cell lines of APEX2-null MEFs were transfected with pcDNA3.1/Hygro(+), pcDNA3.1/Hygro(+):mAPEX2, pIRES1hyg, or pIRES1hyg:mAPEX2 with the aid of LipofectAMINE (Invitrogen) according to the manufacturer's instructions, and stable transfectants were selected in the presence of 300 μg/mL hygromycin B. Expression of recombinant APEX2 protein was confirmed by Western blotting.

Colony formation assay

Exponentially growing MEFs were plated in 10-cm dishes at a density of 500 cells per dish. The cells attached to dishes by incubation for 6 hours were exposed to various doses of x-ray irradiation as described under "X-ray irradiation." Each plate was incubated for 2 more weeks. Formed colonies were stained in 25% ethanol containing 0.3% crystal violet, and counted.

Splenocyte proliferation assay

Splenocytes were prepared from 6-week-old male mice with an *Apex2*$^-$ or *Apex2*$^+$ genotype, treated with acetate kinase lysing buffer (pH 7.4, 150 mM NH_4Cl 10 mM KHCO3, 0.1 mM Na2-EDTA), and suspended in culture medium supplemented with 20 μg/mL lipopolysaccharide (LPS) (from *Escherichia coli*, 055:B5; Sigma, St Louis, MO) or 4 μg/mL concanavalin A (ConA) (Wako, Osaka, Japan) at a cell density of 1.0×10^6/mL. Then, 200 μL cell suspension per well was dispensed in multiple-well plates and cultured for 72 hours. Every 24 hours, the cells from 3 wells subjected to each treatment were harvested, and then viable and dead cells were stained by the trypan blue exclusion method and counted under a microscope.

For cell cycle analysis, 2 mL splenocyte suspension per well was dispensed in a 24-well plate. Cells cultured with LPS or concanavalin A were harvested at 48 hours and 60 hours, respectively. Nuclei were isolated from the harvested cells, and the DNA contents were analyzed as described.[14]

To analyze expression of APEX2 protein, 10 mL splenocyte suspension per dish was placed in 90-mm–diameter dishes (Nunc, Rochester, NY) for 48 hours, and cells were harvested. Whole-cell extracts were prepared and subjected to Western blotting with anti-mAPEX2.

Analysis of the immune response to chicken egg ovalbumin

Eleven-week-old wild-type (n = 6) and APEX2-null mice (n = 6) were immunized with 3 intraperitoneal injections of chicken egg ovalbumin (OVA) (Sigma) (300 μg per injection) on days 0, 21, and 35. Animals were separated into 2 groups, and on alternate weeks, peripheral blood was collected from the tail veins of each group in biweekly sampling. Concentrations of total immunoglobulin M (IgM), IgA, and IgG in serum were analyzed by the single radial immunodiffusion method,[16] and titers of OVA-specific antibodies were determined by an enzyme-linked immunosorbent assay using peroxidase-conjugated anti–mouse IgM (Rockland, Gilbertsville, PA) and anti–mouse IgG (Jackson ImmunoResearch Laboratories, Bar Harbor, ME) antibodies. Peroxidase activities were measured with a Sumilon peroxidase assay kit (Sumitomo Bakelite, Tokyo, Japan), according to the manufacturer's instructions.

Statistical analysis

To determine statistical significance, data of wild-type and APEX2-null mice were analyzed by the Welch *t* test, Mann-Whitney U test, or 2-way analysis of variance (ANOVA) with the use of StatView Software Ver. 5.0 (SAS Institute, Cary, NC).

Results

Growth retardation in APEX2-null mice

Heterozygous female ($Apex2^{+/-}$) mice bearing a mutated *Apex2* (*Apex2*$^-$) allele on an X chromosome, in which a genomic region from the 3′ region of its intron 5 to 5′ region of its exon 6 was replaced with a *neo* cassette,[14] were backcrossed with C57BL/6J males ($Apex2^{+/Y}$). From the backcross, almost equal numbers of wild-type ($Apex2^{+/Y}$) and knock-out ($Apex2^{-/Y}$) males, and wild-type ($Apex2^{+/+}$) and heterozygous females ($Apex2^{+/-}$) were obtained, indicating that the *Apex2* gene is not essential for viability (Table 1). The reverse-transcriptase polymerase chain reaction (data not shown) and Western blot analysis (Figure 1A) confirmed that thymocytes of $Apex2^{-/Y}$ mice are APEX2-null. The APEX2-null male mice showed moderate growth retardation (Figure 1B). Their body weights were about 80% those of the wild-type male littermates at birth, and this tendency persisted into childhood and adulthood (Figure 1C-D), indicating that all developing embryos, infants, and adults of APEX2-null mice may somehow be retarded in growth.

Thymic atrophy

Thymus glands of APEX2-null mice exhibited statistically significant atrophy, and their relative weights were about 50% those of the wild-type thymus (Figure 2A). The total number of thymocytes in APEX2-null thymus decreased to about 20% of that in the wild-type thymus (Figure 2B). Histologic abnormalities in the cortex or medulla of thymi from APEX2-null mice were not apparent, however, APEX2-null thymocytes appeared to be larger than the wild-type cells (Figure 2C). Flow cytometric analysis clearly showed that a fraction of small cells abundant in wild-type thymocytes, which is likely to represent the resting $CD4^+CD8^+$ thymocytes,[17] was largely reduced in the APEX2-null thymocytes (Figure 2D). Propidium iodide staining and flow cytometric analysis of isolated nuclei of thymocytes revealed that populations of APEX2-null thymocytes in both S and G_2/M phases were statistically significantly increased compared with the wild type (Figure 2E), indicating a delayed progression of S phase and increased arrest in G_2/M phase. APEX2-null female mice had essentially identical phenotypes, in terms of growth retardation and thymic atrophy, to those observed in APEX2-null male mice (data not shown).

General dyshematopoiesis

An analysis of peripheral blood cells of 6-week-old mice revealed general and moderate dyshematopoiesis in APEX2-null young mice (Table 2). The number of white blood cells in APEX2-null mice was significantly ($P < .01$) reduced to 42% of the wild-type level, and populations of $CD3^+$ T lymphocytes and $B220^+$ B lymphocytes were 44.8% and 33.3% of the wild-type levels, respectively, although the numbers of red blood cells, $CD11b^+$/$Dx5^-$ monocytes/granulocytes, $Dx5^+/CD3^-$, natural killer cells, but not platelets, were only slightly reduced (Table 2). We also

Table 1. Genotypes of progeny from backcrosses of heterozygous female ($Apex2^{-/+}$, F_1) with wild-type male ($Apex2^{+/Y}$, C57BL/6J) mice

Sex	Genotype, no.		
	WT	Heterozygous	KO
Male	13	0	15
Female	15	15	0

Heterozygous, $Apex2^{-/+}$; KO, $Apex2^{-/-}$ or $Apex2^{-/Y}$.

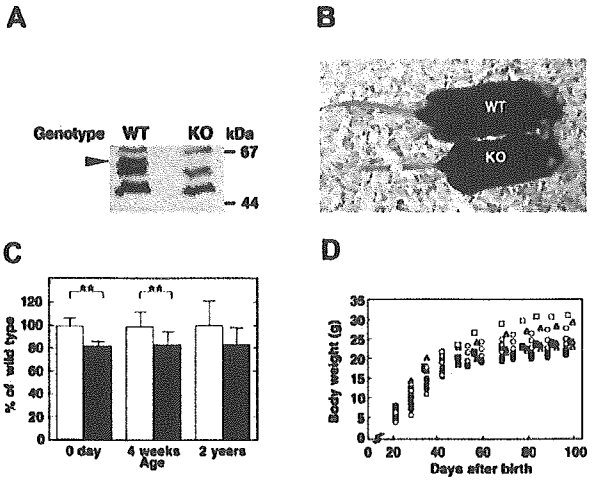

Figure 1. Growth retardation of APEX2-null mice. (A) No APEX2 protein was detected in the *Apex2* KO mouse. Whole-cell extracts of thymocytes from wild-type (WT) and *Apex2* KO mice were prepared. APEX2 protein in extracts was detected by Western blotting using anti-APEX2 antibody as indicated by an arrowhead. (B) Photograph of an F_6 15-week-old APEX2-null male mouse (KO) and its wild-type littermate (WT). Body weights of the KO and WT mice were 19.9 g and 27.2 g, respectively. (C) Mean values ± standard deviation (SD) of body weights of male mice with each genotype at an age of 0 days (F_{10} mice, 7 WT and 12 KO), 4 weeks (F_9 mice, 10 WT and 13 KO), and 2 years (F_3 mice, 12 WT and 7 KO) are shown. Open columns indicate WT; solid columns, KO mice. $^{**}P < .01$. No asterisk indicates not statistically significant ($P > .05$). (D) Growth curves of APEX2-null males and their wild-type littermates. Each symbol tracks the growth of an individual mouse. Littermates with different genotypes are indicated with the same symbol. Open symbols indicate WT; closed symbols, KO mice.

analyzed peripheral blood of 13-week-old adult APEX2-null mice, and observed decreased densities of white and red blood cells as compared with wild-type mice (Table 2). In thymus of 6-week-old APEX2-null mice, most fractions of thymocytes ($CD4^+CD8^+$, $CD4^-CD8^+$, and $CD4^+CD8^-$) were significantly ($P < .01$) reduced to about 20% of the wild-type levels (Table 3), as was observed in 4-week-old APEX2-null mice (Figure 2B). The number of $CD4^-CD8^-$ cells in the APEX2-null thymus was reduced to only 50% of the wild-type level. The relative ratio of $B220^+$ B cells in bone marrow cells was reduced to 75% of the wild-type level, irrespective of IgM expression (Table 4).

Sensitivity to x-ray exposure

After mice were exposed to 1 Gy x-ray irradiation, about 11% of thymocytes in APEX2-null thymus survived, while more than 41% of thymocytes survived in the wild-type mice (Figure 3A). The sub-G_1 fraction appeared in APEX2-null thymocytes 3 hours after the irradiation, but it was not so prominent in the wild type, indicating that APEX2-null thymocytes underwent apoptosis after x-ray exposure (data not shown). To examine whether the increased x-ray sensitivity of APEX2-null thymocytes is a general phenotype for any type of cells, we established immortalized MEFs from 3 APEX2-null embryos and introduced plasmid encoding mouse APEX2 protein to each cell line. Unexpectedly, each APEX2-null MEF line exhibited essentially the same colony-forming efficiency after exposure to various doses of x-ray irradiation, regardless of recombinant APEX2 expression (Figure 3B).

Abnormal proliferation and cell cycle progression of peripheral lymphocytes

To examine whether the defects observed in lymphopoiesis in vivo are cell-autonomous defects, we further analyzed cultured primary

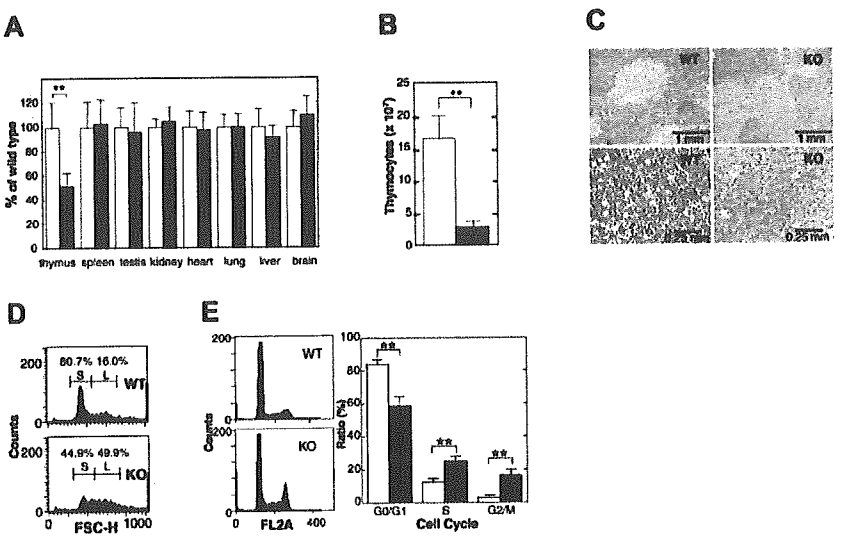

Figure 2. Thymic atrophy in APEX2-null mice. (A) Organ weight. The body weight and weight of each organ of 32- or 33-day-old F_7 male mice were measured, and the weight of each organ was normalized to the body weight of each mouse. The weight of each organ of APEX2-null mice (KO) was expressed relative to the weight of the corresponding organ of wild-type mice (WT) and shown as a percentage ± SD of the WT value. Open columns indicate WT (n = 11); solid columns, KO mice (n = 13). $^{**}P < .01$. No asterisk indicates not statistically significant ($P > .05$) (B) Total number of thymocytes. Means ± SD of the total number of thymocytes in thymus from 4-week-old male mice are shown. Open column indicates WT (n = 7); solid column, KO mice (n = 7). $^{**}P < .01$. (C) Histology. Thin sections of thymi of 4-week-old male mice were fixed with formaldehyde, embedded in paraffin, and stained with hematoxylin and eosin. Left panels are WT; right panels are KO mouse. (D) Flow cytometric analysis of thymocyte sizes. Thymocytes from WT (upper panel) and KO (lower panel) mice were analyzed by flow cytometry. Size distributions of thymocytes represented by forward scatter heights (FSC-Hs) are shown in histograms. Fractions of small and large thymocytes are indicated by S and L, respectively. (E) APEX2-null thymocytes show abnormal progression of the cell cycle. Isolated nuclei were stained with propidium iodide and cell cycle distribution was determined by flow cytometry. Left panels indicate representative histograms of DNA contents in isolated nuclei of thymocytes from WT (n = 7) and KO mice (n = 8). The distribution of isolated nuclei in each cell cycle phase was determined with the use of ModFit software and is shown with SD in the right panel. $^{**}P < .01$.

splenocytes. In the absence of stimulation, splenocytes isolated from both APEX2-null and wild-type spleen were mostly in the quiescent state, and similarly underwent cell death during in vitro culture (Figure 4A). After stimulation with either LPS or ConA, APEX2-null splenocytes started to proliferate, but the extent of proliferation was much less than in wild-type splenocytes. The number of dead cells in the culture of APEX2-null splenocytes was almost equal to that of wild-type splenocytes (data not shown). The relative ratio of APEX2-null cells in G_2/M phase was statistically significantly increased in comparison with the wild type (Figure 4B). Western blot analysis showed a notable induction of APEX2 expression in splenocytes after stimulation with these mitogens (Figure 4C).

Table 2. Moderate dyshematopoiesis in 6- and 13-week-old APEX2-null mice

Age of mice and cell type	Density, counts/μL*	
	Wild type	APEX2-null
6 wks		
WBC†	5400 ± 1095	2275 ± 640
RBC, ×10⁴‡	928 ± 41	771 ± 29
PLT, ×10⁴	60 ± 17	73 ± 25
CD11b⁺/D×5⁻‡	877 ± 338	482 ± 154
D×5⁺/CD3⁻	522 ± 151	391 ± 90
B220⁺†	3064 ± 513	1021 ± 308
CD3⁺†	1440 ± 344	643 ± 179
CD8⁺CD3⁺†	506 ± 109	227 ± 59
CD4⁺CD3⁺†	817 ± 150	345 ± 86
13 wks		
WBC†	6800 ± 748	3640 ± 804
RBC, ×10⁴†	945 ± 42	833 ± 29
PLT, ×10⁴	85 ± 24	105 ± 19

WBC indicates white blood cells; RBC, red blood cells; PLT, platelets,
*The mean ± standard deviation representing at least 5 mice.
†$P < .01$ by Welch t test.
‡$P < .05$ by Welch t test.

Attenuated immune response in APEX2-null mice

To evaluate the ability to produce functional antibodies, we initially analyzed levels of various immunoglobulins in peripheral blood of naive APEX2-null mice. Concentrations of total IgM, IgG, and IgA in peripheral blood of naive APEX2-null mice were essentially the same as in naive wild-type mice (Figure 5A). We then immunized APEX2-null and wild-type mice with OVA and collected peripheral blood from the immunized mice. From around 4 weeks after immunization, titers of anti-OVA IgM and IgG gradually increased in both APEX2-null and wild-type mice (Figure 5B); however, the mean titers of both anti-OVA IgM and anti-OVA IgG in the APEX2-null mice were always lower than those in the wild type, even at 7 weeks after the first immunization. We further immunized an additional 5 APEX2-null and 5 wild-type mice, collected their serum 4 weeks after the first immunization, and analyzed titers of anti-OVA antibodies. Although not of statistical significance ($P > .05$), mean titers of both anti-OVA IgM and anti-OVA IgG of

Table 3. Thymic dyslymphopoiesis in 6-week-old APEX2-null mice

Types of cells†	Cell count, ×10⁵ in thymus*	
	Wild type	APEX2-null
Total cells	1156 ± 125	234 ± 32
CD4⁻CD8⁻	45 ± 7	25 ± 5
CD4⁺CD8⁺	982 ± 128	179 ± 24
CD4⁻CD8⁺	33 ± 3	10 ± 3
CD4⁺CD8⁻	96 ± 8	20 ± 3
CD3⁺	88 ± 14	18 ± 3

*The mean ± standard deviation representing 5 mice.
†$P < .01$ by Welch t test.

Table 4. Decreased population of IgM⁻ B lymphocytes in 6-week-old APEX2-null mice

Type of cells	Percentage in bone marrow cells*	
	Wild type	APEX2-null
B220⁺†	35.2 ± 1.6	26.3 ± 2.2
B220⁺/IgM⁺	14.7 ± 2.2	12.2 ± 0.8
B220⁺/IgM⁻†	20.4 ± 1.4	14.1 ± 2.4

*The mean ± standard deviation representing 5 mice.
†$P < .01$ by Welch t test.

APEX2-null mice were consistently lower than those of wild-type mice, as shown in Figure 5C.

Discussion

APEX2 is highly expressed in mouse thymus, spleen, and bone marrow, consistent with the significant abnormalities in these organs seen in APEX2-null mice.[14] A major AP endonuclease, APEX1, is also highly expressed in these tissues; however, our results indicate that APEX2 deficiencies in these tissues are not compensated for by APEX1. Thus, results of the present study provide the first evidence for the biologic significance of APEX2 in mammals.

B lymphocytes were most severely reduced in peripheral blood of APEX2-null mice. Recently, it was reported that UNG-deficient mice and human patients exhibit abnormalities in immunoglobulin class-switch recombination and in somatic hypermutation in B lymphocytes.[18,19] Nilsen et al[20] reported the hyperplasia of lymphoid organs, including thymus in UNG-null mice; other mice deficient in any DNA glycosylase have never been reported to exhibit such hyperplasia of lymphoid organs. It has been shown that both UNG and APEX2 bind PCNA via their PCNA-binding motives, thus indicating that both play a crucial role during DNA replication or replication-associated BER.[4] It is most likely that lack of UNG results in reduced generation of AP sites while lack of APEX2 in the presence of UNG results in increased accumulation of AP sites. Thus, we suggest that the large number of AP sites in lymphoid cells cause dyslymphopoiesis as we observed in APEX2-null mice, and that dyslymphopoiesis may be suppressed by simultaneous loss of UNG. The fact that the major AP endonuclease, APEX1, could not efficiently compensate for the lack of APEX2 clearly demonstrates the biologic significance of APEX2, especially in lymphoid organs. The highest expression of some other DNA glycosylases, including MUTYH and NEIL3 (endonuclease VIII-like 3), were also detected in thymus.[1,21-23] MUTYH and NEIL3 have a PCNA-binding motif or a topoisomerase III homologous domain, respectively, which they shared in common with APEX2. Thus, we suggest that these DNA glycosylases may generate AP sites that are repaired by APEX2 in thymocytes. The difference in phenotypes of B lymphocytes and thymocytes may be due to accumulation of AP sites generated by UNG, MUTYH, NEIL3, or other DNA glycosylases. We did not observe any histologic abnormality in intestinal epithelium (data not shown), suggesting that the severely altered phenotype in APEX2-null mice is rather specific to lymphopoietic cells.

A decreased population of developing thymocytes as well as an abnormal proliferation of peripheral mature T lymphocytes was apparent in APEX2-null mice. Furthermore, various populations of

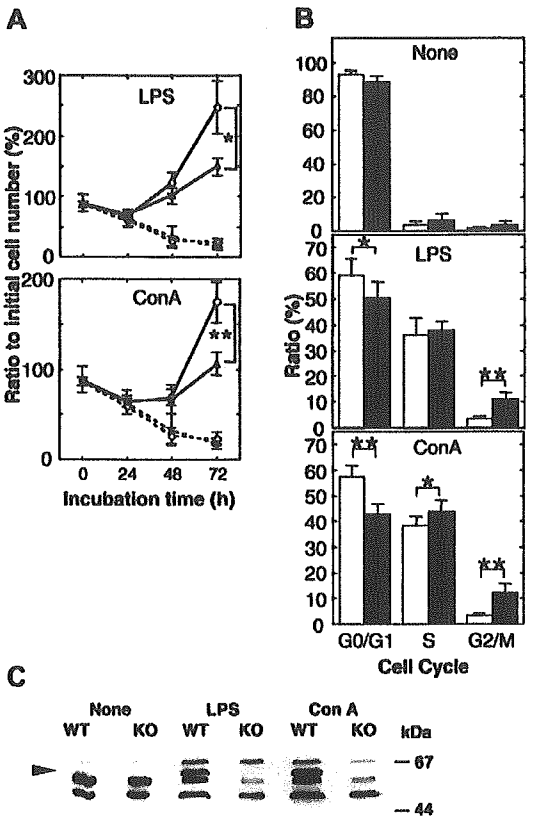

Figure 4. Delayed progression of the cell cycle during proliferation of peripheral lymphocytes. (A) Mitogen-induced proliferation of splenocytes of wild-type (WT, n = 4) and APEX2-null (KO, n = 4) mice. Splenocytes were stimulated with LPS or ConA, and numbers of viable cells were counted under a microscope. Mean values ± SD are indicated. ○ indicates WT; ▲, KO. Solid lines represent cells incubated with mitogens; dotted lines indicate that no stimulant was used. $^{**}P < .01$. $^{*}P < .05$. (B) Cell cycle distribution of proliferating splenocytes. DNA contents of isolated nuclei stained with propidium iodide were analyzed by flow cytometry. Distribution of isolated nuclei in each cell cycle phase is shown as a percentage ± SD. Open columns indicate WT (n = 7); closed columns, KO mice (n = 10). $^{**}P < .01$. $^{*}P < .05$. (C) Induction of APEX2 expression by stimulation with LPS or ConA for 48 hours. APEX2 protein in whole-cell extracts of splenocytes from WT and KO mice was detected by Western blotting using anti-APEX2, as indicated by the arrowhead.

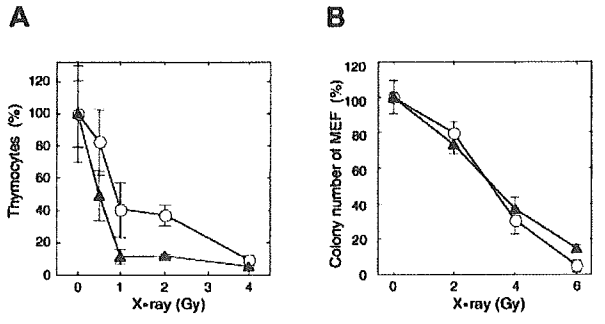

Figure 3. Increased sensitivity of thymocytes of APEX2-null mice to x-ray irradiation. (A) Mice were exposed to various x-ray doses. Thymus glands were collected 21 hours later, and viable thymocytes were counted. Ratios (percentages) of the numbers of thymocytes relative to those of an unirradiated control are shown with their mean values and SD. At least 3 mice were exposed to each x-ray dose. The difference between wild-type and APEX2-null mice was statistically significant ($P = .0006$, 2-way ANOVA). ○ indicates wild type; ▲, APEX2-null. (B) X-ray sensitivity of APEX2-null MEF lines. APEX2-null MEF lines with pIRES1hyg:mAPEX2 (○) or pIRES1hyg (▲) were plated in triplicate at a cell density of 500/10-cm dish and exposed to x-ray irradiation. After culture for 14 days, colonies were stained with crystal violet and counted. Ratios (percentages) of the numbers of colonies relative to those of an unirradiated control are shown with their mean values and SD.

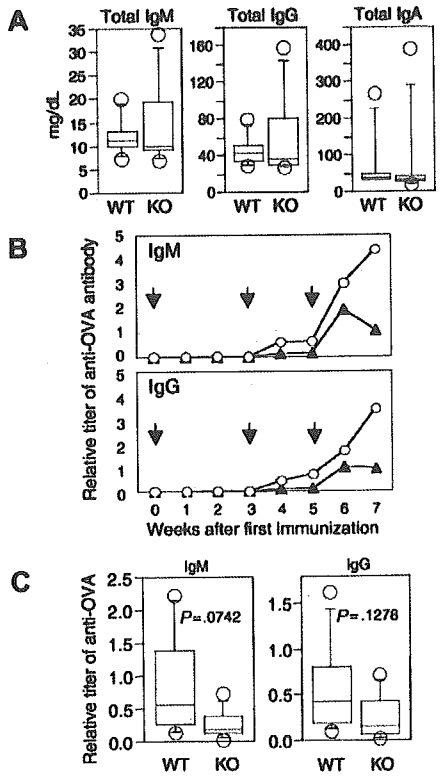

Figure 5. Immunoglobulin levels in peripheral blood of naive and immunized APEX2-null mice. (A) Concentrations of IgM, IgG, and IgA of 11-week-old naive wild-type (WT, n = 7) and APEX2-null mice (KO, n = 8). Concentrations of immunoglobulins in serum are shown with box-and-whisker plots. In each plot, the box is bound top and bottom by upper and lower quartiles, and the statistical median is shown as a horizontal line within the box. The whiskers extend outward from the box to the farthest points that are not outliers (circles). The concentration of each immunoglobulin (IgM, IgG, or IgA) in serum of APEX2-null mice was not significantly different from that of wild-type mice (Mann-Whitney U test, $P > .05$). (B) Time-dependent induction of antigen-specific antibodies in wild-type and APEX2-null mice after immunization with OVA. Eleven-week-old wild-type (n = 6) and APEX2-null (n = 6) mice were immunized with 300 μg OVA on days 0, 21, and 35 as shown by arrows. Animals were separated into 2 groups, and serum was collected biweekly from each group of mice on alternate weeks. The mean titers of anti-OVA IgM and IgG of wild-type mice (○) and APEX2-null mice (▲) are shown as line graphs. (C) OVA-specific antibodies in wild-type and APEX2-null mice immunized with OVA for 4 weeks. A total of 8 mice were immunized with OVA as described in panel B. The titers of their serum anti-OVA IgM and IgG are shown with box-and-whisker plots. Differences between wild-type and APEX2-null mice were not statistically significant (Mann-Whitney U test, $P > .05$).

hematopoietic lineages, which are derived from common stem cells in bone marrow, were significantly decreased in peripheral blood of APEX2-null mice. Thus, our data may suggest that there is an attenuated proliferation of bone marrow stem cells as well as abnormality in peripheral mature blood cells of APEX2-null mice.

Using spontaneously immortalized or simian virus 40 (SV40) T antigen-immortalized APEX2-null MEF lines, we analyzed their sensitivity to various DNA-damaging agents such as hydrogen peroxide, bleomycin, or x-ray irradiation; however, any protective effect of endogenous APEX2 in wild-type MEF lines or recombinant APEX2 protein expressed in all APEX2-null MEF lines was not evident (Figure 3B; also D.T., Y.I., Y.N., unpublished results, December 2002). Furthermore, after hydrogen peroxide challenge, we did not observe any difference in survival between APEX2-null and wild-type mouse embryonic stem cell lines.[14] Thus, it is likely that APEX1 but not APEX2 plays major role in base excision repair against such DNA damaging agents in these cell lines, suggesting that APEX2 function is selectively required for proper cell cycle progression of activated T cells and B cells. The increased population of proliferating lymphocytes in both S and G_2/M phases in APEX2-null mice suggests that an APEX2 deficiency increases the obstacles to be overcome for progression of the cell cycle. APEX2 but not APEX1 would be required in replication-associated BER to incise AP sites in the nascent strand because of the ability of APEX2 to bind PCNA. Thus, the lack of APEX2 most likely results in a delayed progression of replication-associated BER. We hypothesize 2 models for a mechanism of replication-associated BER. The first is a replication-coupled BER, in which misincorporated bases such as uracil or adenine opposite 8-oxoguanine are repaired immediately after their incorporation by replicative DNA polymerases. The other is a postreplicative BER, in which misincorporated bases left behind replication forks are repaired before completion of S phase. In either model, the inefficient PCNA-anchored BER machinery itself might be an obstacle to DNA replication and cause delayed S phase and G_2/M phase arrest. We did not detect any increased apoptosis in thymocytes and stimulated splenocytes, and this may indicate that the remaining AP sites in APEX2-null cells are likely to be slowly repaired by APEX1. It has been reported that *Saccharomyces cerevisiae* also possesses a APEX2 homolog, Apn2.[24] Recently, Guillet et al[25] reported that an *S cerevisiae* mutant strain lacking *apn1*, *rad1*, *ung1*, and *apn2*, which possesses decreased AP endonuclease activities, exhibits growth delay owing to a G_2/M checkpoint arrest. Our data observed in APEX2-null mice are in good agreement with the phenotype.

After immunization with OVA, production of anti-OVA antibodies in APEX2-null mice was somehow retarded in comparison with wild-type mice. Notably, anti-OVA IgG was apparently induced in APEX2-null mice as well as anti-OVA IgM, indicating that immunoglobulin class-switch recombination (CSR) was achieved. UNG, in addition to its general role in replication-associated BER, is thought to play a specific role in CSR by excising the uracil base produced by activation-induced cytidine deaminase (AID).[18,19] This function of UNG might be independent of PCNA because generation of uracil base in DNA by AID should be independent of DNA replication. APEX2 is the PCNA-associated AP endonuclease, and thus may participate in replication-associated BER initiated by UNG or other DNA glycosylases, but not in the AID-initiated CSR during which UNG produces AP sites independent of PCNA.

An APEX2 deficiency in mice is not lethal and may be associated with certain human hereditary diseases. The human *APEX2* gene is also located on the X chromosome[9]; thus, a mutation in one *APEX2* allele of a germ line might easily lead to the birth of APEX2-deficient male offspring. The human diseases anticipated from an APEX2 deficiency might be more prevalent in males and be associated with decreased body size, moderate immunodeficiency, and a high sensitivity of lymphocytes to x-ray irradiation.

Acknowledgments

We thank M. Furuichi and H. Sumichika for their helpful discussions; A. Matsuyama, S. Kitamura, J. Ikeda, and Y. Yamada for their technical assistance; and W. Campbell for comments on the manuscript.

References

1. Nakabeppu Y, Tominaga Y, Tsuchimoto D, et al. Mechanisms protecting genomic integrity from damage caused by reactive oxygen species: implications for carcinogenesis and neurodegeneration. Environ Mutagen Res. 2001;23:183-195.
2. Friedberg EC, Walker GC, Siede W. DNA Repair and Mutagenesis. Washington, DC: American Society for Microbiology; 1995.
3. Parker A, Gu Y, Mahoney W, Lee SH, Singh KK, Lu AL. Human homolog of the MutY repair protein (hMYH) physically interacts with proteins involved in long patch DNA base excision repair. J Biol Chem. 2001;276:5547-5555.
4. Otterlei M, Warbrick E, Nagelhus TA, et al. Post-replicative base excision repair in replication foci. EMBO J. 1999;18:3834-3844.
5. Hayashi H, Tominaga Y, Hirano S, McKenna AE, Nakabeppu Y, Matsumoto Y. Replication-associated repair of adenine:8-oxoguanine mispairs by MYH. Curr Biol. 2002;12:335-339.
6. Nilsen H, Rosewell I, Robins P, et al. Uracil-DNA glycosylase (UNG)-deficient mice reveal a primary role of the enzyme during DNA replication. Mol Cell. 2000;5:1059-1065.
7. Seki S, Ikeda S, Watanabe S, et al. A mouse DNA repair enzyme (APEX nuclease) having exonuclease and apurinic/apyrimidinic endonuclease activities: purification and characterization. Biochim Biophys Acta. 1991;1079:57-64.
8. Hadi MZ, Wilson DM 3rd. Second human protein with homology to the Escherichia coli abasic endonuclease exonuclease III. Environ Mol Mutagen. 2000;36:312-324.
9. Tsuchimoto D, Sakai Y, Sakumi K, et al. Human APE2 protein is mostly localized in the nuclei and to some extent in the mitochondria, while nuclear APE2 is partly associated with proliferating cell nuclear antigen. Nucleic Acids Res. 2001;29:2349-2360.
10. Demple B, Herman T, Chen DS. Cloning and expression of APE, the cDNA encoding the major human apurinic endonuclease: definition of a family of DNA repair enzymes. Proc Natl Acad Sci U S A. 1991;88:11450-11454.
11. Robson CN, Hickson ID. Isolation of cDNA clones encoding a human apurinic/apyrimidinic endonuclease that corrects DNA repair and mutagenesis defects in E. coli xth (exonuclease III) mutants. Nucleic Acids Res. 1991;19:5519-5523.
12. Xanthoudakis S, Curran T. Identification and characterization of Ref-1, a nuclear protein that facilitates AP-1 DNA-binding activity. EMBO J. 1992;11:653-665.
13. Xanthoudakis S, Smeyne RJ, Wallace JD, Curran T. The redox/DNA repair protein, Ref-1, is essential for early embryonic development in mice. Proc Natl Acad Sci U S A. 1996;93:8919-8923.
14. Ide Y, Tsuchimoto D, Tominaga Y, Iwamoto Y, Nakabeppu Y. Characterization of the genomic structure and expression of the mouse Apex2 gene. Genomics. 2003;81:47-57.
15. Oda S, Nishida J, Nakabeppu Y, Sekiguchi M. Stabilization of cyclin E and cdk2 mRNAs at G1/S transition in Rat-1A cells emerging from the G0 state. Oncogene. 1995;10:1343-1351.
16. Vergani C, Stabilini R, Agostoni A. Quantitative determination of serum immunoglobulins by single radial immunodiffusion on cellulose acetate. Immunochemistry. 1967;4:233-237.
17. Ernst B, Surh CD, Sprent J. Thymic selection and cell division. J Exp Med. 1995;182:961-971.
18. Rada C, Williams GT, Nilsen H, Barnes DE, Lindahl T, Neuberger MS. Immunoglobulin isotype switching is inhibited and somatic hypermutation perturbed in UNG-deficient mice. Curr Biol. 2002;12:1748-1755.
19. Imai K, Slupphaug G, Lee WI, et al. Human uracil-DNA glycosylase deficiency associated with profoundly impaired immunoglobulin class-switch recombination. Nat Immunol. 2003;4:1023-1028.
20. Nilsen H, Stamp G, Andersen S, et al. Gene-targeted mice lacking the Ung uracil-DNA glycosylase develop B-cell lymphomas. Oncogene. 2003;22:5381-5386.
21. Nishioka K, Ohtsubo T, Oda H, et al. Expression and differential intracellular localization of two major forms of human 8-oxoguanine DNA glycosylase encoded by alternatively spliced OGG1 mRNAs. Mol Biol Cell. 1999;10:1637-1652.
22. Ohtsubo T, Nishioka K, Imaiso Y, et al. Identification of human MutY homolog (hMYH) as a repair enzyme for 2-hydroxyadenine in DNA and detection of multiple forms of hMYH located in nuclei and mitochondria. Nucleic Acids Res. 2000;28:1355-1364.
23. Morland I, Rolseth V, Luna L, Rognes T, Bjoras M, Seeberg E. Human DNA glycosylases of the bacterial Fpg/MutM superfamily: an alternative pathway for the repair of 8-oxoguanine and other oxidation products in DNA. Nucleic Acids Res. 2002;30:4926-4936.
24. Johnson RE, Torres-Ramos CA, Izumi T, Mitra S, Prakash S, Prakash L. Identification of APN2, the Saccharomyces cerevisiae homolog of the major human AP endonuclease HAP1, and its role in the repair of abasic sites. Genes Dev. 1998;12:3137-3143.
25. Guillet M, Boiteux S. Origin of endogenous DNA abasic sites in Saccharomyces cerevisiae. Mol Cell Biol. 2003;23:8386-8394.

Blockade of Vascular Endothelial Growth Factor Suppresses Experimental Restenosis After Intraluminal Injury by Inhibiting Recruitment of Monocyte Lineage Cells

Kisho Ohtani, MD; Kensuke Egashira, MD, PhD; Ken-ichi Hiasa, MD; Qingwei Zhao, MD; Shiro Kitamoto, MD; Minako Ishibashi, MD; Makoto Usui, MD; Shujiro Inoue, MD; Yoshikazu Yonemitsu, MD; Katsuo Sueishi, MD; Masataka Sata, MD; Masabumi Shibuya, MD; Kenji Sunagawa, MD

Background—Therapeutic angiogenesis by delivery of vascular endothelial growth factor (VEGF) has attracted attention. However, the role and function of VEGF in experimental restenosis (neointimal formation) after vascular intraluminal injury have not been addressed.

Methods and Results—We report herein that blockade of VEGF by soluble VEGF receptor 1 (*sFlt-1*) gene transfer attenuated neointimal formation after intraluminal injury in rabbits, rats, and mice. *sFlt-1* gene transfer markedly attenuated the early vascular inflammation and proliferation and later neointimal formation. *sFlt-1* gene transfer also inhibited increased expression of inflammatory factors such as monocyte chemoattractant protein-1 and VEGF. Intravascular VEGF gene transfer enhanced angiogenesis in the adventitia but did not reduce neointimal formation.

Conclusions—Increased expression and activity of VEGF are essential in the development of experimental restenosis after intraluminal injury by recruiting monocyte-lineage cells. (***Circulation.* 2004;110:2444-2452.)

Key Words: restenosis ■ remodeling ■ inflammation ■ endothelium-derived factors ■ gene therapy

Vascular endothelial growth factor (VEGF) has attracted attention for endothelial regeneration and angiogenesis.[1–3] VEGF is one of the most potent vascular permeability factors known, is thought to function as an endogenous regulator of endothelial integrity after injury, and thus, protects the artery from disease progression.[4] Previous animals studies have reported that local delivery of VEGF after endothelial injury promotes endothelial regeneration, accelerates the recovery of endothelium-dependent relaxation, and reduces neointimal formation (see review[4]), suggesting the close correlation between accelerated endothelial integrity and reduced neointima after balloon injury. Increased expression of VEGF and its 2 receptors (VEGFR-1, Flt-1; VEFGR-2, Flk-1) in atherosclerotic and restenotic lesions has been reported.[5–7] However, there is still considerable debate over the vasculoprotective versus atherogenic effects of VEGF.[8] Emerging evidence suggests that (1) VEGF induces migration and activation of monocytes[9]; (2) VEGF induces adhesion molecules[10] and monocyte chemoattractant protein-1 (MCP-1)[11]; and (3) VEGF enhances neointimal formation and atherogenesis by stimulating intraplaque angiogenesis in hypercholesterolemic animals without balloon injury[12,13] or by increasing monocyte infiltration into atherosclerotic lesions.[14] Therefore, it remains unclear whether VEGF protects the artery from vascular disease or accelerates vascular disease.

See p 2283

Clinical and experimental studies involving arterial gene transfer of VEGF showed that it failed to reduce restenosis after balloon angioplasty.[15–17] The role of VEGF in restenotic changes (neointimal formation and negative remodeling) after injury therefore remains a mystery. This is mainly because the inhibitor of VEGF has not been tested for experimental restenosis, although inhibitors of VEGF are currently being evaluated for tumor angiogenesis and other treatment-intractable inflammatory disorders.[3] It is practically impossible to investigate the role of VEGF in postnatal life in mice lacking VEGF or its receptors, because the absence of VEGF function leads to embryonic lethality owing to vascular defects.[4] A soluble form of the VEGF receptor-1 (sFlt-1) is expressed endogenously by vascular endothelial cells and can inhibit VEGF activity by directly sequestering VEGF and by functioning as a dominant-negative inhibitor against VEGF.[18] We and others have demonstrated that intramuscular transfection of the *sFlt-1* gene effectively and specifically

Received June 18, 2004; revision received August 14, 2004; accepted August 20, 2004.

From the Departments of Cardiovascular Medicine (K.O., K.E., M.U., Q.Z., S.K., M.I., K.-i.H., S.I., K.S.) and Pathology (Y.Y., S.K.), Graduate School of Medical Sciences, Kyushu University, Fukuoka; the Department of Cardiovascular Medicine (M. Sata), Graduate School of Medical Sciences, University of Tokyo, Tokyo; and the Division of Genetics (M. Shibuya), Institute of Medical Science, University of Tokyo, Tokyo, Japan.

An online-only Data Supplement is available at http://www.circulationaha.org

Correspondence to Kensuke Egashira, MD, PhD, Department of Cardiovascular Medicine, Graduate School of Medical Science, Kyushu University, 3-1-1, Maidashi, Higashi-ku, Fukuoka 812-8582, Japan. E-mail egashira@cardiol.med.kyushu-u.ac.jp

Circulation **is available at http://www.circulationaha.org**

DOI: 10.1161/01.CIR.0000145123.85083.66

blocks VEGF and thus, "quenches" the activity of VEGF in remote organs in vivo.[19,20]

The aim of this study was to decisively determine a role for VEGF in restenotic changes after intraluminal injury. We report herein that blockade of VEGF by systemic *sFlt-1* gene transfer attenuates the development of neointimal formation after intraluminal injury by inhibiting inflammation, which suggests an essential role for VEGF in the pathogenesis of restenosis after injury. Our present data are clinically important because VEGF gene therapy for therapeutic angiogenesis and restenosis has been attempted in clinical studies.[16,17,21]

Methods

Expression Vector

The 3.3-kb mouse *sFLT-1* gene, originally obtained from the mouse lung DNA library,[22] was cloned into the *Bam*HI (5′) and *Not*1 (3′) sites of the eukaryotic expression vector plasmid cDNA3 (Invitrogen). Plasmid cDNA3 encoding the luciferase gene was used to detect gene transfection.

Rat and Rabbit Models of Balloon Injury

The study protocol was reviewed and approved by the Committee on Ethics on Animal Experiments, Kyushu University Faculty of Medicine, and the experiments were conducted according to the guidelines of American Physiological Society. A portion of this study was performed at the Kyushu University Station for Collaborative Research.

Twenty-week-old male, normal chow–fed Wistar-Kyoto rats were anesthetized, and their right common carotid arteries were injured by passage (3 times) of an infiltrated 2F Fogarty balloon catheter.[23] Male Japanese white rabbits weighing 3.0 to 3.5 kg were fed a high-cholesterol diet for 2 weeks. Their right common carotid arteries also were injured by passage (3 times) of an inflated 2F Fogarty catheter.[24] After injury, all rabbits were fed the same high-cholesterol diet. Three days before balloon injury, the animals were randomly divided into 2 groups: the empty-plasmid group was injected with the empty plasmid, and the *sFlt-1* group was injected with the *sFlt-1* gene into femoral muscle (150 μg/50 μL TE buffer [10 mmol/L Tris-HCl, 1 mmol/L EDTA, pH 8.0] in rats, 1500 μg/0.5 mL TE buffer in rabbits). To enhance transgene expression, all plasmid-injected animals received electroporation at the injection site immediately after injection with an electric pulse generator (CUY21, BTX) as previously described.[19,23–25]

Morphometric and Immunohistochemical Analyses

All animals were euthanized by intravenous injection of a lethal dose of sodium pentobarbital. Tissue sections from rabbits and rats were prepared as described[23,24] and either (1) stained with Masson's trichrome or elastica van Gieson's stains or (2) subjected to immunostaining with antibodies against macrophages/monocytes (ED1, Serotec, for rats; RAM11, Dako, for rabbits), proliferating cells (proliferating cell nuclear antigen for rats from Dako, Ki-67 for rabbits from Dako), endothelial cells (CD31, Dako), VEGF (Santa Cruz), VEGFR-1 (Santa Cruz), VEGFR-2 (Santa Cruz), α-smooth muscle actin (Dako), MCP-1 (R&D Systems), interleukin-1β (IL-1β; R&D Systems), or nonimmune mouse IgG (Zymed). After avidin-biotin amplification, the slides were incubated with diaminobenzidine and counterstained with hematoxylin. Immunofluorescence double staining was performed to localize VEGF and its receptors by the use of fluorescence-conjugated antibodies in rats. Morphometric analysis was performed by microscopy with a computerized digital image-analysis system by a single observer who was blinded to the treatment protocol.[23,24]

Real-Time Quantitative Reverse Transcription–PCR

Real-time polymerase chain reaction (PCR) amplification was performed with rabbit cDNA by using the ABI PRISM 7000 sequence detection system (Applied Biosystems) as described previously.[23] The respective PCR primers and TaqMan probes were designed from GenBank databases aided by a software program (Applied Biosystems; online Table I). Results were analyzed by sequence detection software (Applied Biosystems), expressed in arbitrary units, and adjusted for glyceraldehyde 3-phosphate dehydrogenase mRNA levels.

Mouse Femoral Wire-Injury Model With Bone Marrow Reconstitution

Intraluminal injury of the femoral artery of wild-type mice whose bone marrow had been replaced with that of ROSA26 mice, which expresses β-galactosidase (LacZ) ubiquitously, was performed.[26] Four weeks after bone marrow transplantation, transluminal arterial injury was induced by inserting a straight spring wire (0.38 mm in diameter) into the femoral artery as described.[26] The femoral artery was excised and stained with X-gal solution for 7 hours and then fixed in 4% paraformaldehyde. LacZ-positive cells were counted and expressed as a proportion of the total number of cells. The paraffin-embedded sections were stained with elastica van Gieson's stain.

Peripheral blood was obtained from the retro-orbital venous plexus of the mice. Fluorescence-conjugated antibodies against CD31 (Pharmingen) and c-Kit (Pharmingen) were used as bone marrow–derived monocyte-lineage markers. A fluorescein isothiocyanate–conjugated antibody against Mac-1 (Pharmingen) was used as a circulating monocyte-lineage marker after gating for monocyte cell size with exclusion of granulocytes. Data were analyzed by flow cytometry and appropriate software (Becton Dickinson).

Blood Measurements

Plasma total cholesterol levels in rabbits were determined with commercially available kits (Wako Pure Chemicals). To measure sFlt-1 released by the transfected skeletal muscle, plasma concentrations of sFlt-1 were measured by use of an sFlt-1 ELISA kit (R&D Systems) in rabbits. Concentrations of VEGF in plasma and femoral arterial tissues were also measured in mice by use of an ELISA kit (R&D Systems).

Statistical Analysis

Data are expressed as mean±SE. Statistical analysis of differences was compared by ANOVA and Bonferroni's multiple-comparison tests. A level of $P<0.05$ was considered statistically significant.

Results

Increased Expression of VEGF and Its Receptors in Rabbits and Rats

Significant increases in VEGF mRNA levels were detected after balloon injury in rabbits, which peaked on day 7 and persisted until day 28 (Figure 1A). Immunohistochemical staining revealed that VEGF and VEGFR-1 increased in vascular smooth muscle cells in the media and regenerated endothelial layer during the early phase (day 7) and in cells in the neointima, media, and adventitia during the later phase (day 28) after balloon injury in rabbits (Figure 1B). VEGFR-2 did not increase on day 7 but did increase in the injured artery on day 28. *sFlt-1* gene transfer reduced the increased immunoreactivities of VEGF, VEGFR-1, and VEGFR-2 on day 28 (Figure 1B).

The localization of VEGF, VEGFR-1, and VEGFR-2 was studied in rats by immunohistochemistry. As observed in rabbits, immunoreactive VEGF and VEGFR-1 increased in the media on days 3 and 7 and in the neointima, media, and adventitia on day 28 (Figure 2A). The increase in immunoreactive VEGFR-2 was less prominent during the early phase but became apparent on day 28 (Figure 2A).

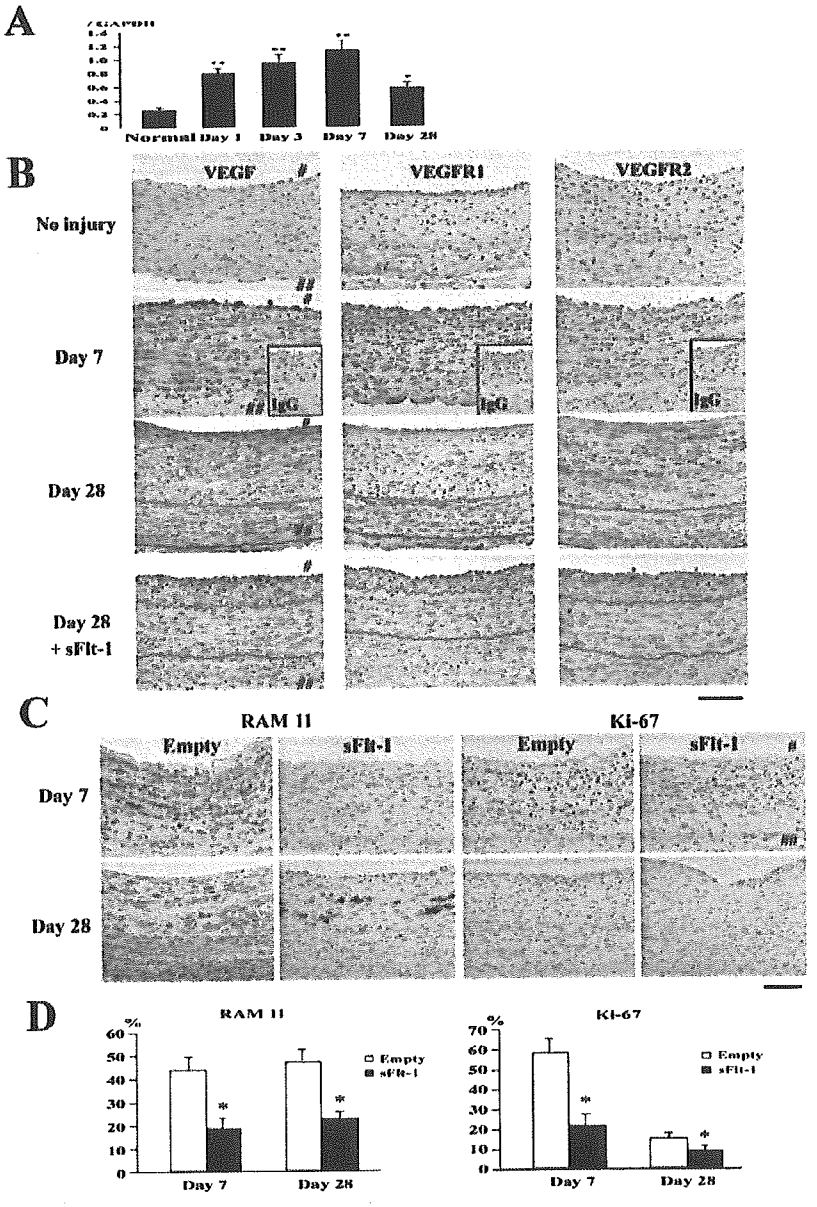

Figure 1. Expression of VEGF after balloon injury and inhibitory effects of *sFlt-1* gene transfer on inflammatory-proliferative changes in rabbits. A, Time course of VEGF mRNA levels in rabbits. mRNA levels were assessed by real-time PCR at indicated times. Expression of VEGF mRNA in each sample was normalized to glyceraldehyde 3-phosphate dehydrogenase mRNA expression in that sample. Each bar has n=6 to 8. $^{*}P<0.05$, $^{**}P<0.01$ vs control (uninjured) artery. B, Immunohistochemistry of rabbit carotid artery. Arterial cross sections were stained immunohistochemically with VEGF, VEGFR-1 (Flt-1), VEGFR-2 (Flk-1), or nonimmune IgG. # and ## indicate lumen and adventitia, respectively. Internal and external elastic layers are highlighted with blue and black lines, respectively, in photographs taken 28 days after injury. Bar indicates 100 μm. C, Carotid artery sections from empty-plasmid and *sFlt-1* groups 7 and 28 days after balloon injury were stained immunohistochemically with antibody against monocytes/macrophages (RAM11) or proliferating cells (Ki-67). # and ## indicate lumen and adventitia, respectively. Bar=100 μm. D, Effect of *sFlt-1* gene transfer on inflammation (RAM11-positive monocytes/macrophages) and proliferation (Ki-67–positive cells) 7 and 28 days after balloon injury (n=8 each). $^{*}P<0.01$ vs control group.

Fluorescence double immunohistochemistry revealed that VEGF and VEGFR-1 were expressed predominantly in α-smooth muscle actin–positive cells in the media and neointima on day 28 (Figure 2B). During the early phase, ED1-positive monocytes recruited into the intima and adventitia expressed VEGFR-1 but not VEGFR-2 (Figure 2C). *sFlt-1* gene transfer reduced the increased immunoreactivities of VEGF, VEGFR-1, and VEGFR-2 on day 28 (data not shown).

Inhibitory Effects of *sFlt-1* Transfer on Inflammatory and Proliferative Changes in Rabbits

As we reported,[23,24] inflammatory and proliferative changes became evident by 3, 7, and 28 days after balloon injury in rabbits (Figure 1C and 1D). *sFlt-1* gene transfer reduced these inflammatory and proliferating changes.

Inhibitory Effects of *sFlt-1* Transfer on Neointimal Formation and/or Negative Remodeling in Rabbits and Rats

The carotid arteries in the control and empty-plasmid groups developed significant neointimal formation and negative remodeling (smaller lumen size, internal elastic lamina, and external elastic lamina) in rabbits by day 28 (Figure 3A and 3B). The arteries from the *sFlt-1* group showed less neointimal formation, negative remodeling, perivascular fibrosis, and adventitial vasa vasorum; an adventitial VEGFR-2–positive vasa vasorum; and a larger lumen area. There was no significant difference in plasma levels of total cholesterol between the 2 groups (online Table II), indicating that the observed effects of *sFlt-1* gene transfer were not caused by changes in serum cholesterol levels. In rats, neointimal

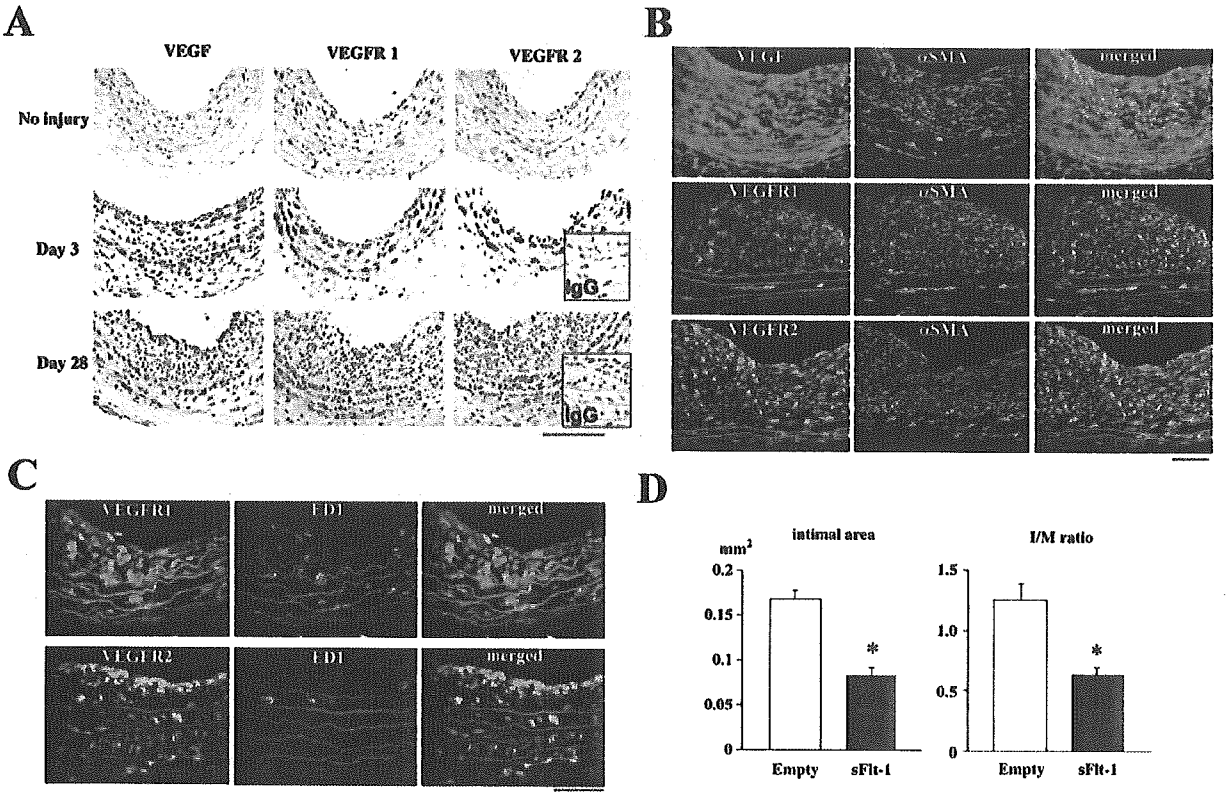

Figure 2. Expression of VEGF and its receptors after balloon injury and inhibitory effects of *sFlt-1* gene transfer on neointimal formation in rats. A, Immunohistochemistry of arterial cross-sections stained immunohistochemically with VEGF, VEGFR-1 (Flt-1), or VEGFR-2 (Flk-1). Bar indicates 100 μm. B, Fluorescence double immunohistochemistry 28 days after balloon injury. Photomicrographs show injured arteries stained with VEGF, VEGF-R1 (Flt-1), or VRGFR-2 (Flk-1) in green. Photomicrographs show injured arteries also stained with α-smooth muscle actin in red. Single-fluorescence–positive cells were stained in green or red, whereas double-positive cells were stained in yellow. Scale bar indicates 100 μm. C, Fluorescence double immunohistochemistry 7 days after balloon injury. Photomicrographs show injured arteries stained with VEGF-R1 or VEGF-R2 in green. Photomicrographs show injured arteries also stained with ED1 in red. Single-fluorescence–positive cells were stained in green or red, whereas double-positive cells were stained in yellow. Scale bar indicates 100 μm. D, Neointimal formation (neointimal area and intima-media ratio) on 28 day after balloon injury. *P<0.01 vs empty-plasmid group, n=8 or 9.

formation was also less in the *sFlt-1* group than in the empty-plasmid group on day 28 (Figure 2D).

To assess transfection efficacy of *sFlt-1*, plasma sFlt-1 concentration was measured in rabbits. The plasma sFlt-1 levels were 96±14, 377±25 (P<0.01 versus before), 413±20 (P<0.01), 284±15 (P<0.05), and 113±16 (P>0.1) pg/mL before and at 3, 7, 14, and 28 days after *sFlt-1* transfection, respectively, indicating that sFlt-1 was released from the transfected muscle to the circulation.

No Significant Effects of *sFlt-1* Gene Transfer on Endothelial Regeneration in Rabbits and Mice

In rabbits, there were no significant differences between the empty-plasmid and *sFlt-1*–transfected groups in the ratio of luminal surface area covered with endothelium (Figure 4A) and that of the CD31-positive endothelial layer 7 days after injury (Figure 4B). In mice, endothelial recovery was scarcely observed on day 7 (data not shown) but was noted equally in the 2 groups on day 14 (Figure 4C).

Inhibitory Effects of *sFlt-1* Transfer on Expression of Proinflammatory Factors

sFlt-1 transfection reduced the increased gene expression of MCP-1, platelet-derived growth factor, transforming growth factor-β, IL-1β, IL-6, tumor necrosis factor-α, matrix metalloproteinase-9, and VEGF (Figure 5A). *sFlt-1* transfer did not affect the increased gene expression of matrix metalloproteinase-1 and tissue factor. Immunohistochemical staining performed 7 days after balloon injury revealed increased immunoreactive MCP-1 and IL-1β in cells in the neointima and smooth muscle cells in the media, which were attenuated by *sFlt-1* gene transfer (Figure 5B).

Contribution of Bone Marrow Cells to the Effect of *sFlt-1* Gene Transfer in Mice

As reported,[26] a considerable proportion of neointimal and medial cells were LacZ-positive 28 days after injury in mice whose bone marrow expressed LacZ ubiquitously. Intimal area, intima-media ratio, and LacZ-positive cells were decreased in *sFlt-1*–transfected mice than in empty plasmid–